Development and evaluation of 0.05° terrestrial water storage estimates using CABLE land surface model and GRACE data assimilation

Natthachet Tangdamrongsub [1,2], Michael F. Jasinski [2], Peter Shellito [1,2]

5 [1] Earth System Science Interdisciplinary Center, University of Maryland, College Park, Maryland, USA
[2] Hydrological Sciences Laboratory, NASA Goddard Space Flight Center, Greenbelt, Maryland, USA

Correspondence to: Natthachet Tangdamrongsub (natthachet.tangdamrongsub@nasa.gov)

Abstract. Accurate estimation of terrestrial water storage (TWS) at a meaningful spatiotemporal resolution is important for reliable assessments of regional water resources and climate variability. Individual components of TWS include soil moisture,

10 snow, groundwater, and canopy storage and can be estimated from the Community Atmosphere Biosphere Land Exchange (CABLE) land surface model. The spatial resolution of CABLE is currently limited to 0.5° by the resolution of soil and vegetation datasets that underlie model parameterizations, posing a challenge to using CABLE for hydrological applications at a local scale. This study aims to improve the spatial detail (from 0.5° to 0.05°) and timespan (1981 – 2012) of CABLE TWS estimates using rederived model parameters and high-resolution meteorological forcing. In addition, TWS observations

15 derived from the Gravity Recovery and Climate Experiment (GRACE) satellite mission are assimilated into CABLE to improve TWS accuracy. The success of the approach is demonstrated in Australia, where multiple ground observation networks are available for validation. The evaluation process is conducted using four different case studies that employ different model spatial resolutions and include or omit GRACE data assimilation (DA). We find that the CABLE 0.05° developed here improves TWS estimates in terms of accuracy, spatial resolution, and long-term water resource assessment

20 reliability. The inclusion of GRACE DA increases the accuracy of groundwater storage (GWS) estimates and has little impact on surface soil moisture or evapotranspiration. The use of improved model parameters and improved state estimations (via GRACE DA) together is recommended to achieve the best GWS accuracy. The workflow elaborated in this paper relies only on publicly accessible global datasets, allowing reproduction of the 0.05° TWS estimates in any study region.

1 Introduction

25 Accurate knowledge of terrestrial water storage (TWS) is crucial for assessing water resource and climate variability (Delworth, and Manabe, 1988; Koster and Suarez, 2001). TWS consists of soil moisture, groundwater, snow, and canopy storage. Each component plays a significant role in the global water cycle and interacts closely with the land-atmospheric water-energy exchange (Koster et al., 2006; Fischer et al., 2007; Seneviratne et al., 2010). The TWS components can be measured or estimated by various platforms (e.g., satellite measurement, model simulation). However, spatial resolutions are

30   relatively coarse due to the limitation of sensors and models that primarily focus on global or continental scales (e.g., Rodell et al., 2004, Alkama et al., 2010). At a regional or local scale, the spatial resolution of the TWS estimate is vital, as most applications (e.g., risk management for drought or flood) require accurate information at the county or sub-county level (Quiring, 2009). This motivates the development of TWS estimates at more meaningful spatiotemporal scales, corresponding particularly to an increased interest in exploiting TWS in interdisciplinary studies (e.g., IPCC 2007; NASEM, 2018).

35   TWS information can be obtained or estimated from ground observation networks, satellite measurements, or model simulations. Each has different strengths and limitations. Ground observations (e.g., soil moisture probe, groundwater well) are considered the most reliable, providing measurements closest to the truth (e.g., Dorigo et al., 2013). However, ground observations have high maintenance costs and incomplete coverage. Also, point measurements only reflect information at one location, not necessarily the entire region. On the other hand, satellite platforms offer an automated measurement with

40   improved coverage ranging from regional to global (e.g., Tapley et al., 2004; Entekhabi et al., 2010a). The challenges of using satellite measurements are the coarse spatial resolution and the sensors' technical limitations (e.g., penetration depth, cloud/vegetation obstruction, background noise). Therefore, its usage is restricted to a sufficiently large region and requires a sophisticated algorithm to retrieve TWS variables (Crow et al., 2012; Castellazzi et al., 2016; Tangdamrongsub et al., 2019). In addition, satellite measurements can be limited by a relatively short period of record.

45   TWS components can also be simulated from a land surface model (LSM) such as the Community Atmosphere Biosphere Land Exchange (CABLE, Kowalczyk et al., 2006; Decker 2015). CABLE is a core LSM of the Australian Community Climate and Earth System Simulator (ACCESS, Bi et al., 2013; Kowalczyk et al., 2013). The LSM incorporates various land surface physics into complex numerical sequences to allow the simulation of TWS to be performed at any desired location and spatiotemporal scale (Pitman 2003). The LSM can provide a complete suite of TWS components compared with the ground

50   or satellite measurements that can only measure a single or integrated TWS component (e.g., Tapley et al., 2004; Entekhabi et al., 2010a). However, due to the limitations of input data, the spatial resolution of many LSMs is coarse (e.g., > 25 km), which consequently restricts its application to a sufficiently large region (e.g., Rodell et al., 2004; Alkama et al., 2010; Ke et al., 2012). For CABLE, the spatial scale is currently limited to the 0.5° (~50 km) resolution of model parameter and forcing datasets (Decker 2015; Ukkola et al., 2016; Haverd et al., 2018). Models and their inputs must be reconfigured to increase the

55   spatial detail of TWS estimates for smaller-scale studies (e.g., 5 – 10 km).

Efforts to improve the spatial resolution (and timespan) of global TWS estimates have been made in many modeling communities (e.g., Wood et al., 2011; Bierkens et al., 2014; Bierkens, 2015). For instance, Ke et al. (2012) improved the resolution of the Community Land Model (CLM) from ~50 km to ~5 km using modified land surface parameters. The World-Wide Water model (W3, van Dijk et al., 2013) recently allows the global TWS variables to be estimated at ~ 5 km (see

60   http://wald.anu.edu.au/challenges/water/w3-and-ozwald-hydrology-models, last access: 16 February 2020). The European Centre for Medium-Range Weather Forecasts (ECMWF) Reanalysis 5 (ERA5) offers global land surface variables at ~ 10 km resolution from 1981 to present (https://confluence.ecmwf.int/display/CKB/ERA5-Land%3A+data+documentation, last

access: 14 October 2020). A similar effort is also seen in hydrologic model development, such as the PCRaster Global Water

Balance (PCR-GLOBWB; Sutanudjaja et al., 2018), which improves the spatial resolution from ~50 km to ~10 km and extends

65 the timespan to more than a 50-year period. The enhancement of model spatial resolution and timespan receives even more

attention at the local level, where spatial detail down to a few km is needed (e.g., Tesfa et al., 2014; Rasmussen et al., 2014;

Singh et al., 2015; Beamer et al., 2016; Dong et al., 2020). The effort to increase the regional or local study's spatial resolution

has not been considered thus far for CABLE.

On top of the improved spatiotemporal resolution, the improved accuracy of TWS estimates is also a concern in LSM

70 developments. As in most environmental modeling systems, model outputs are associated with a high degree of uncertainty

propagated from, e.g., inaccurate meteorological forcings, imperfect model physics, and ineffective parameter calibration. Data

assimilation (DA, Reichle et al., 2002; Reichle 2008) techniques can be employed to improve LSM performance. The approach

sequentially updates the model's states using an optimal value computed by combining model simulations with observations.

A variety of satellite observations reflecting different TWS components can be assimilated into the system (e.g., Kumar et al.,

75 2014; Dong et al., 2018). TWS observations from the Gravity Recovery And Climate Experiment (GRACE) satellite mission

(Tapley et al., 2004) offer integrated water column information that can be used to constrain multiple water storage components

simultaneously (e.g., Zaitchik et al., 2008; Forman et al., 2012; Tangdamrongsub et al., 2015). GRACE DA has shown positive

impacts on most TWS components, including groundwater (e.g., Girotto et al., 2017; Nie et al., 2019), soil moisture (Jung et

al., 2019), and snow (Kumar et al., 2016).

80 This study aims to improve the accuracy, spatial resolution, and timespan of CABLE TWS estimates. Our approach utilizes

only publicly available global datasets, so resulting TWS estimates can be reproduced over any target region (see Data

availability section for the data access). The spatial detail of CABLE is improved from 0.5° to 0.05° (~5 km) using high-

resolution forcing data (precipitation in particular) and land surface parameters derived from high-resolution maps of soil and

vegetation cover. The development is demonstrated in Australia, where ground observation networks (e.g., surface soil

85 moisture, groundwater, and evapotranspiration) are available to validate the result. The demonstrated simulation period is 1981

– 2012, coincident with the availability of meteorological forcing data. The GRACE mascon solution (Luthcke et al., 2013) is

assimilated into the model to improve the accuracy of TWS components between 2003 and 2012. Assimilating the coarse

GRACE observations into a much higher-resolution model is performed using the 3-dimension ensemble Kalman smoother

(EnKS 3D; Tangdamrongsub et al., 2017).

90 The objectives of this paper are 1) to present the development and evaluation of retrospective 0.05° TWS estimates, and 2) to

assess the GRACE DA impact on both 0.5° and 0.05° CABLE versions, as well as the benefit of assimilating the coarse

resolution satellite data into a fine-scale model. This paper is presented as follows. Sect. 2 provides the details of the study

area, model configurations, and data processing. Sect. 3 presents the GRACE DA schematic and the statistical metric used in

the evaluation. Sect. 4 presents the assessment and validation of the result. Finally, Sect. 5 summarizes the findings of this

95 study and provides a possible direction for future development.

2 Study area and data

2.1 Study area

This study uses Australia as a case study. Due to its size and geographic location, Australia is influenced by multiple climate drivers (Murphy and Timbal, 2008; Xie et al., 2016) and experiences episodes of severe droughts and floods (e.g., van Dijk et al., 2013). The recent long-term drought, known as the Millennium Drought (Bond et al., 2008), severely affects industrial and agricultural sectors and has led to a significant economic loss nationwide (see, e.g., van Dijk et al., 2013). The need for an accurate prediction of possible water scarcity from climate variations motivated the development of land surface and hydrology models in Australia, e.g., the Australian Water Availability Project (AWAP; Raupach et al., 2008), the Australian Water Resources Assessment - Landscape Model (AWRA-L; van Dijk 2010), and CABLE (Kowalczyk et al., 2006). Recent work has assimilated GRACE satellite data into such water models (e.g., Tian et al., 2017; Schumacher et al., 2018; Tangdamrongsub et al., 2020). Studies relevant to GRACE DA in Australia are summarized in Table 1. Ground observation networks have also been installed across the continent and continuously monitor the water storage and flux variations. Such data records are valuable for validating the accuracy of the model estimates and remote sensing observations. Details regarding the in situ data used in this study are provided in Sect. 2.3.2.

(Please insert Table 1 here)

2.2 Model configuration

In this study, TWS estimates are derived from CABLE. A history of the model's development can be found in, e.g., Wang et al. (2011), Kowalczyk et al. (2013), Decker (2015), Haverd et al., (2018). Multiple CABLE versions have been developed since 2003 for different objectives (see https://trac.nci.org.au/trac/cable/wiki/CableCommunity); CABLE SubgridSoil GroundWater (CABLE-SSGW; Decker, 2015) is considered most suitable for our uses due to its inclusion of comprehensive terrestrial water storage components, especially a groundwater module. The model has been used to simulate global TWS at 0.5° spatial resolution using 0.5°-resolution model parameters and forcing data (e.g., Decker, 2015; Ukkola et al., 2016). The variables used to assess TWS consist of soil moisture storage (SMS), snow water equivalent (SWE), canopy storage (CNP), and groundwater storage (GWS).

The model parameters of CABLE-SSGW are derived from several different sources (Kowalczyk et al., 2006; Wang et al., 2011; Decker, 2015). Land use/vegetation type categories are obtained from the International Global Biosphere Project (IGBP) classification from the Moderate Resolution Imaging Spectroradiometer (MODIS; Friedl et al., 2002). Relative volumes of silt, sand, clay, and organic matter in the soil are obtained from the Harmonized World Soil Database (Fischer et al., 2008). The Zobler soil category (Zobler, 1999) is computed empirically from the silt, sand, and clay fractions (Oleson et al., 2010). The monthly climatology of the leaf area index (LAI) is computed using a reprocessed MODIS LAI product (Yuan et al.,

2011). All derived model parameters are resampled to 0.5° to match the 0.5° model grid space. Comprehensive details of model parameters can be found in, e.g., Kowalczyk et al. (2006), Wang et al. (2011), and Decker (2015).

This study also rederives the model parameters and employs enhanced forcing data to increase the model spatial detail from 0.5° to 0.05°. The vegetation type is derived from the global land cover climatology using MODIS data (Broxton et al., 2014).
130 The soil map is still derived from the Harmonized World Soil Database but at 0.05° grid spacing. The 0.05° monthly climatology LAI is derived from the Global Land Surface Satellite product (GLASS; Xiao et al., 2013). All rederived parameters are shown in Fig. 1. The soil layer thicknesses from top to bottom are set to 1.2, 3.8, 25, 39.9, 107.9, 287.2 cm, and the unconfined aquifer's thickness is set to 20 m. The surface soil moisture (SSM, m^3/m^3) is defined as the top two layers, and the SMS (m) is computed from all soil layers.

135   (Please insert Figure 1 here)

The CABLE model is forced with precipitation, air temperature, wind speed, humidity, surface pressure, and shortwave and longwave downward radiation. For precipitation, we use the Climate Hazards Group InfraRed Precipitation with Station data (CHIRPS; Funk et al., 2015), provided on a 0.05° grid. The other forcing variables are provided on a 0.5° grid by the high-resolution global dataset of meteorological forcings for land surface modeling version 2, Princeton University (Princeton,
140 Sheffield et al., 2006). When performing 0.5° model simulations, the CHIRPS data is spatially averaged to 0.5° grid space while other forcing variables maintain their intrinsic 0.5° resolution. When performing 0.05° model simulations, the coarser-resolution forcing variables are spatially resampled to 0.05° model grid space using nearest-neighbor interpolation.

Model simulations are performed between 1981 and 2012 (total 32 years), given the Princeton forcing data's availability. Similar to McNally et al. (2017), temporal disaggregation is applied to CHIRP precipitation data to resample from 1 day to 3
145 hours, consistent with the Princeton data's time step. The scale factor derived from the 3-hour Princeton precipitation data is used to (temporally) rescale the CHIRPS data. The characteristics of forcing data and the derived model parameters used in this paper are given in Table 2.

                          (Please insert Table 2 here)

In all simulations, initial states are obtained using a 320-year spinup, i.e., performing ten repeated runs between 1981 and
150 2012.

2.3 GRACE data

GRACE is a twin satellite-to-satellite tracking mission designed to measure the mean and time-varying components of the Earth's gravity field (Tapley et al., 2004). Every month, GRACE provides a time-varying gravity solution containing information about mass redistribution near the Earth's surface. The monthly gravity change is dominated by a hydrology signal,
155 making the GRACE product beneficial for various hydrological and geophysical applications (e.g., Klees et al., 2008; Mouyen et al., 2018, Rodell et al., 2018; Tapley et al., 2019). Different GRACE solutions have been released (see, e.g.,

https://podaac.jpl.nasa.gov/GRACE or http://icgem.gfz-potsdam.de), including the mascon solution (e.g., Luthcke et al., 2008; Rowlands et al., 2010). The mascon approach utilizes mass concentration blocks (as a basis function) to determine the Earth's mass variation and is found to provide a more accurate TWS estimate as compared with the spherical harmonic approach

160 (Rowlands et al., 2010). In this study, the mascon product from the Goddard Space Flight Center (GSFC) is used (Luthcke et al., 2013; https://earth.gsfc.nasa.gov/geo/data/grace-mascons). The GSFC-Mascon product contains monthly TWS variations (ΔTWS), expressed in equivalent water height (in, e.g., m). The glacial isostatic adjustment correction is applied using the ICE6G model (Peltier et al., 2015). The mascon varies in size and represents the average ΔTWS of the associated grid cell. The spatial distribution of mascon in Australia is shown in Fig. 2. The GSFC-Mascon product also provides monthly ΔTWS

165 uncertainties, and they are used to represent the observation error of the individual mascon. To convert monthly ΔTWS into absolute TWS (necessary for the GRACE DA process), the temporal mean value of the CABLE-simulated TWS from 2003 to 2012 is added to the GSFC-Mascon product. This process reconciles the observed long-term mean with the model estimates.

(Please insert Figure 2 here)

2.4 Evaluation data

170 ### 2.4.1 Satellite-derived products

The satellite-derived soil moisture and evapotranspiration (ET) data obtained from the European Space Agency - Climate Change Initiative program (ESA-CCI; Dorigo et al., 2017; Gruber et al., 2019) and the Global Land Evaporation Amsterdam Model (GLEAM; Martens et al., 2017) are used to validate the soil moisture and evaporation estimates, respectively. The ESA-CCI COMBINED product combines multiple active and passive satellite-sensor soil moisture products and provides a near-

175 global daily volumetric soil moisture product at 0.25° resolution with ~0.04 m^3/m^3 accuracy (unbiased root-mean-square error). The combined product version 4.7 (v04.7) is used in this study. The product includes approximately eight different satellite observations, including, e.g., SSM/I., AMSR-E, ASCAT, Windsat, and SMOS (see, e.g., Fig. 3 of Dorigo et al. (2017) for complete details) during our evaluation period (1981 – 2012). GLEAM is an algorithm that derives the daily global terrestrial evaporation using observations from multiple satellite microwave sensors and reanalysis datasets (Martens et al., 2017). Two

180 product variants are available: the satellite-only and the reanalysis, and the newest release of the latter (version 3.3a) is used in this study due to its consistent timespan with our evaluation period.

2.4.2 In situ data

In situ soil moisture, groundwater, and ET measurements are obtained from different ground observation networks. The daily in situ soil moisture data are obtained from the Scaling and Assimilation of Soil Moisture and Streamflow (SASMAS; Rüdiger

185 et al., 2007) network in the southeastern part of the Murray-Darling Basin. The SASMAS network hosts more than twenty measurement sites and provides volumetric soil moisture (θ, m^3/m^3) data associated with 0 – 5 cm depth. Only sites with a data record longer than three years are used in our analysis.

The monthly in situ groundwater level data are collected from the Australian Bureau of Meteorology through the Australian Groundwater Explorer (http://www.bom.gov.au/water/groundwater/explorer/map.shtml). More than 870,000 monitoring bores are distributed unevenly across the continent. At each bore, the groundwater level measurement is converted to the groundwater level variation by removing the long-term mean associated with the entire data record. The bores are excluded from the analysis if the data record is shorter than three years or having significant missing data. The groundwater level measurements are not converted to groundwater storage due to the absence of accurate knowledge of specific yield.

The in situ ET (i.e., latent heat flux) is obtained from the FLUXNET2015 dataset (Pastorello et al., 2017). FLUXNET is a global network measuring carbon and energy fluxes. More than twenty flux tower sites are distributed across Australia associated with different periods (e.g., 2001 – 2014). Only the sites with three years of data or longer are used in our analysis (see site locations in Fig. 1a).

3 Methods

3.1 Ensemble Kalman Smoother (EnKS)

The Ensemble Kalman Smoother (EnKS; Evensen, 2003; Zaitchik et al., 2008) is used to assimilate the GRACE-derived ΔTWS into the CABLE model. The 3-dimension EnKS (EnKS 3D) scheme described in Tangdamrongsub et al. (2017) is used in this study. The GRACE DA comprises forecast, analysis, and distributing update steps. The forecast step propagates the model states forward in time for approximately one month. The analysis step computes the monthly model state update using GRACE observations (and uncertainties). The final step reinitializes the ensemble (e.g., initial states, forcing data) and reperforms the forecast step with the DA update (increment) distributed evenly throughout the month. Figure 3 illustrates the concept of the GRACE DA process.

(Please insert Figure 3 here)

The meteorological forcings and model parameters are perturbed using $N = 100$ ensemble members prior to GRACE DA processing. Multiplicative white noise is used to perturb the precipitation and shortwave radiation, while additive white noise is used for the air temperature and model parameters. The characteristics of the uncertainties are given in Table 3. After the perturbation process, CABLE model states are then propagated for approximately one month (the forecast step). The state vector consists of nine model states ($n = 9$): six soil moisture layers, canopy storage, snow water equivalent, and groundwater storage.

(Please insert Table 3 here)

In the analysis step, when a GRACE observation is available, the monthly averaged states ($\boldsymbol{\psi}$) are related to the GRACE observations by

$$d_j = \mathbf{H}\psi_j + \epsilon_j; \ \epsilon \sim \mathcal{N}(\mathbf{0}, \mathbf{R}), \tag{1}$$

where d_j is an $m \times 1$ perturbed observation vector containing the perturbed GRACE mascon for the month of interest, $\mathbf{H}$ is a measurement operator which relates the ensemble state ψ_j to the vector d_j, m is the number of GRACE mascon cells used in the calculation, and j indicates ensemble index. The uncertainties in the observations are described by the random error ϵ, which is assumed to have zero mean and covariance matrix $\mathbf{R}_{m \times m}$. The subscription denotes the dimension of the matrix. Note that $\mathbf{R}$ is a variance matrix here as only the variance components are provided in the mascon product.

In EnKS 3D, multiple model and observation grid cells (e.g., inside 300 km radius corresponding to GRACE spatial resolution) are simultaneously used to compute the state update. Figure 2 (see circle B) demonstrates the model and mascon grid cells used in the analysis step to compute the update of the center mascon cell (see also Fig. 7 of Tangdamrongsub et al. (2017) for more details). The $\mathbf{H}$ matrix is defined as:

$$\mathbf{H} = \left[\begin{pmatrix} \frac{1}{k_1}(1\ 1\ 1\ \dots\ 1)_{1 \times nk_1} & 0 & \cdots & 0 \\ 0 & \frac{1}{k_2}(1\ 1\ 1\ \dots\ 1)_{1 \times nk_2} & \cdots & 0 \\ \vdots & \vdots & \ddots & \vdots \\ 0 & 0 & \cdots & \frac{1}{k_m}(1\ 1\ 1\ \dots\ 1)_{1 \times nk_m} \end{pmatrix} \right]_{m \times \sum_{i=1}^{m} nk_i} \tag{2}$$

where k_i is the number of model grid cells inside a mascon i (see, e.g., rectangle A in Fig. 2 for the distribution of model grids inside a mascon cell).

The ensemble of the states is stored in a matrix $\mathbf{A}_{K \times N} = (\psi_1, \psi_2, \psi_3, \dots, \psi_N)$, where $K = \sum_{i=1}^{m} nk_i$, and the ensemble perturbation matrix is defined as $\mathbf{A}' = \mathbf{A} - \bar{\mathbf{A}}$, where the matrix $\bar{\mathbf{A}}$ contains the mean values computed from all ensemble members. Similarly, the perturbed GRACE observation vector is stored in the matrix $\mathbf{D}_{m \times N} = (d_1, d_2, d_3, \dots, d_N)$. The analysis equation is then expressed as

$$\mathbf{A}^a = \mathbf{A} + \Delta \mathbf{A} = \mathbf{A} + \mathcal{K}(\mathbf{D} - \mathbf{HA}), \tag{3}$$

with

$$\mathcal{K} = \mathbf{P}_e \mathbf{H}^T (\mathbf{H} \mathbf{P}_e \mathbf{H}^T + \mathbf{R}_e)^{-1}, \tag{4}$$

where $\mathbf{A}^a_{K \times N}$ represents the updated state vector, $\Delta \mathbf{A}_{K \times N}$ is the monthly averaged update from EnKS 3D and $\mathcal{K}_{K \times m}$ is the Kalman gain matrix. The superscript T denotes a transpose (matrix) operator. The model and observation error covariance matrix $(\mathbf{P}_e)_{K \times K}$, $(\mathbf{R}_e)_{m \times m}$ are computed as

$$\mathbf{P}_e = \mathbf{A}'(\mathbf{A}')^T/(N-1), \tag{5}$$

$$\mathbf{R}_e = \mathbf{YY}^T/(N-1), \tag{6}$$

where $\mathbf{Y}$ contains the measurement error of all ensemble members. After the monthly averaged update $\Delta\mathbf{A}$ is obtained, the daily increment ($\Delta\mathbf{A}_d$) of the update is computed by dividing $\Delta\mathbf{A}$ by the total number of days in that month. Note that only $\Delta\mathbf{A}_d$ of the center mascon is saved (see also Tangdamrongsub et al., 2017). The processes described in Eq. (1) – Eq. (6) are

245 repeated through all mascon cells to obtain all individual $\Delta\mathbf{A}_d$ in the study domain. Then, the model is reinitialized using the previous month's initial states, and the simulation is performed again while adding $\Delta\mathbf{A}_d$ to the model initial states daily (the distributing update step). The DA process is performed until the last month of the study period (December 2012).

3.2 Assessment metrics and experiment designs

3.2.1 Resample approach

250 The state estimates are validated against the referenced data described in Sect. 2.3. As the spatial resolution of the model estimate and referenced data are different, a spatial resample is performed before the comparison. The model estimate is resampled to the observation grid space using the nearest neighbor-gridded interpolation when model's resolution is coarser. Conversely, the estimate is upscaled (spatial averaging) when the model's resolution is higher. The evaluation is conducted at the observation grid cell.

255 3.2.2 Correlation and root mean square difference

The agreement between the estimated variable and the in situ data is assessed using the Pearson correlation coefficient (ρ) and the root mean square difference (RMSD). At a particular grid cell, ρ is calculated as:

$$\rho = E[(\boldsymbol{y} - \overline{\boldsymbol{y}})(\boldsymbol{x} - \overline{\boldsymbol{x}})]/(\sigma_y\sigma_x),\tag{7}$$

where the $\boldsymbol{y}$ vector contains the model estimates, the $\boldsymbol{x}$ vector contains the validation data (observations), $E[\ ]$ is the

260 expectation operator, and ($\overline{\boldsymbol{y}},\overline{\boldsymbol{x}}$) and ($\sigma_y,\sigma_x$) are the mean and standard derivations of $\boldsymbol{y}$ and $\boldsymbol{x}$, respectively. The RMSD is computed as:

$$RMSD = \sqrt{\sum(\boldsymbol{y} - \boldsymbol{x})^2/L},\tag{8}$$

where L denotes the length of the time series.

3.2.3 Long-term trend and seasonal variations

265 The long-term trend, annual amplitude, and phase of the time series are computed using the least-squares adjustment associated with five parameters, offset (a), long-term trend (b), annual variation (c, d), and semi-annual variation (e, f). A time series ($\boldsymbol{y}$) at a particular grid cell can be expressed as:

$$\boldsymbol{y} = a + b\boldsymbol{t} + c\sin\omega\boldsymbol{t} + d\cos\omega\boldsymbol{t} + e\sin 2\omega\boldsymbol{t} + f\cos 2\omega\boldsymbol{t},\tag{9}$$

$$\omega = 2\pi/T, \tag{10}$$

where the t vector contains time, and T is an annual period. The annual amplitude ($\mathcal{A}$) and phase (φ) are computed as:

$$\mathcal{A} = \sqrt{c^2 + d^2}, \tag{11}$$

$$\varphi = \arctan_2(c, d). \tag{12}$$

3.2.4 Spatial resolution

The spatial resolution can be determined from the empirical (and isotropic) covariance function (C) computed as (Tscherning and Rapp, 1974):

$$C(\psi_{hk}) = \sum \boldsymbol{p}_h \boldsymbol{p}_l / n_{hl}, \tag{13}$$

where ($\boldsymbol{p}_h, \boldsymbol{p}_l$) are vectors containing data points (h,l) associated with the spherical distance ψ_{hl}, and n_{hl} is the number of data pairs considered in the calculation. The spatial resolution (or correlation length of the covariance function) is defined in this study as the distance ψ at which $C(\psi = 0)$ decreases by half. The diagram in Fig. 4 illustrates how this correlation length is determined.

(Please insert Figure 4 here)

3.2.5 Case studies

This paper uses four case studies to quantify the effect of different model grid size and GRACE DA. The case studies are described as follows:

1. CABLE 0.5°: CABLE model simulations at 0.5° grid size without GRACE DA
2. CABLE 0.05°: CABLE model simulations at 0.05° grid size without GRACE DA
3. GRACE DA 0.5°: CABLE model simulations at 0.5° grid size with GRACE DA
4. GRACE DA 0.05°: CABLE model simulations at 0.05° grid size with GRACE DA

It is noteworthy that the 0.5° or 0.05° represents the CABLE grid size, which may differ from the spatial resolution. The term "spatial resolution" used in this paper refers to the determined resolution computed from Sect. 3.2.4.

4 Results and discussions

4.1 Estimation of TWS components from CABLE simulations (without GRACE DA)

4.1.1 Improvement in spatial resolution

The resolution improvements can be seen by comparing CABLE 0.5° TWS estimates against those from CABLE 0.05°. Both

295 are open-loop (OL) simulations, meaning the model is run without data assimilation. The simulation period is from January
1981 to December 2012. After obtaining TWS estimates, the TWS annual amplitude and phase are computed using Eq. (11 –
12) and are shown in Fig. 5. Both CABLE versions have similar spatial features, but more localized and much finer details are
seen in the CABLE 0.05° simulation than in the CABLE 0.5° simulation. A clear difference in annual amplitude is shown over
the Yarra Ranges and the Alpine National Parks (see Fig. 5a vs. 5b insets). CABLE 0.05° provides greater details of the ΔTWS

300 spatial distribution, and the annual amplitude is approximately 30% higher than it is in the coarse-scale version. Differences
in spatial details are also seen in the phase estimates (see Fig. 5c vs. 5d).

(Please insert Figure 5 here)

The spatial resolutions can be quantitatively determined using the empirical covariance function, Eq. (13), described in Sect.
3.2.4. The covariance function is computed for each month's TWS estimates using all grid points in Australia. Figure 6 shows

305 the averaged spatial resolution (correlation length) of CABLE 0.5° and CABLE 0.05° for each month between 1981 and 2012.
The CABLE 0.5° simulations have a spatial resolution of ∼ 50 km, consistent with the grid size of the input 0.5° CABLE
parameters and forcing data. Larger correlation lengths are found during the rainy seasons: Jan – Apr (in the North) and Aug
– Nov (in the South). These results are in line with the TWS's phase estimates in Fig. 5c and 5d. The soil store or aquifer is
likely filled during the wet seasons leading to a more uniform (and smoother) spatial feature to a certain extent. The use of

310 CABLE 0.05° significantly improves the spatial resolution by about a factor of two to three. It is noted that the spatial resolution
of CABLE 0.05° presented in Fig. 6 reflects the continental averaged value while the finer (higher) spatial resolution is
observed in the individual river basin (not shown).

(Please insert Figure 6 here)

4.1.2 Assessment of long-term TWS variations

315 This study's timespan allows for an assessment of overall trends and decadal variations of TWS estimates. The long-term
trends of water balance states and fluxes from CABLE 0.05° between 1981 and 2012 are shown in Fig. 7. A strong relationship
between components is observed, particularly in the storage components (Fig. 7a – 7d). The TWS and GWS (Fig. 7a and 7d)
have very similar spatial patterns, where a wetting trend is observed in the northern region, the Indian Ocean Basin, and the
western part of the Murray-Darling Basin (see Fig. 1a for the basin's location), and a drying trend is seen in the central part of

320 the continent, the South West Coast Basin, and several parts of the Murray-Darling Basin. The similarity between the TWS
and GWS (both spatially and in magnitude) indicates that GWS is a primary driver of the TWS trend in Australia. By contrast,

soil moisture stores show different spatial patterns: increases in soil moisture are also found in the central and western parts of the continent (Fig. 7c). The SMS generally accommodates a large portion of the seasonal variation in water storage in Australia (see Sect. 4.2), but its role in the long-term trend is marginal, smaller than that of the GWS by about a factor of two. ET trend estimates show a similar spatial pattern to SSM trends (Fig. 7e vs. 7b), which may be explained by ET pulling moisture from SSM stores. The long-term trend of the total runoff is in line with the TWS/GWS, increasing in the North and decreasing in the southeastern region and Tasmania (e.g., Fig. 7f vs. 7a). In the northern region, the soil moisture or aquifer is likely saturated due to a wet climate, with more significant annual rainfall (than the South) by about a factor of five (not shown). Such a condition leads to a greater magnitude of root zone moisture, groundwater recharge, and surface runoff variations. The opposite scenario is observed in the southeastern region, where the depleted TWS/GWS (induced by droughts) likely reduces runoff generation, resulting in a negative runoff trend.

(Please insert Figure 7 here)

Regional water balance components can also be analyzed at interannual and decadal timescales. Figure 8 shows the trends of water balance components in three different decades, 1981 – 1990, 1991 – 2002, and 2003 – 2012. The long-term trends are not monotonic. In other words, there are no "always dry" or "always wet" regions observed between 1981 and 2012. Reversals between increasing and decreasing trends are apparent in all components. For example, northern and western Australia experiences a drying trend between 1981 and 1990 (Fig. 8a) and recovers between 1991 and 2002 (Fig. 8b) after receiving continuously increased rainfall (not shown). The region experiences another drought episode (van Dijk et al., 2013) in the first half of the 2000's, causing decreased water storage between 2003 and 2012 (Fig. 8c). A similar reversal is also seen in the eastern regions: wetting in 1981 – 1990, drying in 1991 – 2002, and wetting again in 2003 – 2012 (Fig. 8a – 8c).

(Please insert Figure 8 here)

Without such a long record, assessment of water resources may have limited reliability. For instance, based only on the ~10-year period of GRACE observations, it is difficult to determine whether the negative TWS trend in western Australia (e.g., Fig. 8c; see also Fig. 11d) is caused by anthropogenic or natural processes (e.g., Richey et al., 2015). Evaporation or runoff after the extremely wet conditions prior to 2002 may also produce a similar decreasing trend (e.g., van Dijk et al., 2011; Munier et al., 2012). By assessing the historical TWS time series of the North-Western Plateau Basin obtained from CABLE 0.05° (Fig. 9), the observed negative trend is more likely governed by a decadal cycle of drought and recovery. This approach demonstrates that there is clear value in utilizing a longer timespan of TWS estimates and can offer a more reliable assessment of regional water resources and climate variations.

(Please insert Figure 9 here)

4.1.3 Comparison with the satellite products

TWS, SSM, and ET estimates are compared with satellite data from GRACE, ESA-CCI, and GLEAM, respectively (see Sect. 2.2 and 2.3 for each product's description). Note that the remote sensing products may contain biases (caused by, e.g., background model, processing algorithm) and do not necessarily represent the truth. (Ground truth validation is performed in Sect. 4.3.) The inter-comparison performed in this section is only to assess the consistency between two independent estimates: model and satellite. The CABLE estimate is rescaled to the satellite product's grid before comparison, as described in Sect. 3.2.1. Figure 10 shows the correlation and RMSD estimates between CABLE 0.5°/CABLE 0.05° results and the evaluated satellite data. On average, both CABLE results are in good agreement with the satellite products, with correlation values greater than 0.55 (see Fig. 10a, 10b, 10e, 10f, 10i, 10j). CABLE 0.05° shows more robust agreement with satellite-derived variables than does CABLE 0.5°; correlation values with TWS, SSM, and ET are 14%, 14%, and 7% higher (respectively) in the former simulations than in the latter. Similar improvements are also observed in the RMSD evaluations, where CABLE 0.05° provides smaller RMSD values than CABLE 0.5° by 4% (TWS), 14% (SSM), and 17% (ET). CABLE 0.05° reduces the RMSD of the SSM estimate to as low as ~0.03 m^3/m^3, e.g., over the South West Coast and Lake Eyre basins, and the average RMSD value in Australia is ~0.06 m^3/m^3. It is worth noting that the average unbiased RMSD value (Entekhabi et al., 2010b) is 0.037 m^3/m^3 (not shown), in line with the accuracy of the CCI product (see, e.g., Table 1 of Dorigo et al. (2017)).

(Please insert Figure 10 here)

The improved agreement between CABLE 0.05° estimates and the satellite products is also seen in the temporal variation (Fig. 11). Compared with the CABLE 0.5° results, CABLE 0.05° increases the dynamic range of the TWS estimates in most basins leading to closer alignment with GRACE observations (Fig. 11a – 11c). Similar increases in the agreement are also observed in the CABLE 0.05° SSM and ET estimates (Fig. 11d – 11i). The observed improvement may be attributed in part to the rederived model parameters. For example, in the North West Plateau Basin, CABLE 0.05° uses a ~17 % higher area-averaged sand fraction than does CABLE 0.5°, which allows faster infiltration/drainage in the storage compartments leading to greater dynamic ranges of TWS and SSM variations (see Fig. 11a and 11d). Consequently, the ET estimate is decreased as a response to increased water storage following the water balance equation (Fig. 11g). Similar mechanisms are also observed in Lake Eyre and South West Coast Basins, where the improved parameterization leads to improved agreement with the satellite data. The use of coarse resolution forcing data (e.g., precipitation) could also explain the small TWS amplitude observed in CABLE 0.5°. Coarse scale forcing data averages local precipitation signals over a larger area than does the finer resolution forcing data, resulting in a smaller amplitude.

(Please insert Figure 11 here)

4.2 The impact of GRACE DA

GRACE observations are assimilated into the CABLE 0.5° and CABLE 0.05° models (called GRACE DA 0.5° and GRACE DA 0.05°, respectively) between January 2003 and December 2012 (with respect to the availability of meteorological forcing and GRACE data). The basin-averaged TWS estimates from CABLE with and without GRACE DA are shown in Fig. 12, alongside the GRACE observations themselves. In most basins, apparent disagreements between the open-loop estimates and the GRACE observations suggest the current CABLE models' limited accuracy. After assimilating GRACE into the models, the estimates (GRACE DA 0.5° and GRACE DA 0.05°) move toward the GRACE observations. The positive impact of GRACE DA on the basin-averaged TWS estimates is similar regardless of the model spatial resolutions. This likely reflects the nature of GRACE observations that provide integrated water storage information at continental or basin-scale (Tapley et al., 2004). However, it should be noted that the GRACE DA application does not degrade the spatial resolution of the model. The offline analysis shows that the average correlation length of GRACE DA 0.5° and GRACE DA 0.05° remain the same as that of CABLE 0.5° and CABLE 0.05°, respectively (not shown). The EnKS 3D scheme exploits the spatially correlated information from the high-resolution model to disaggregate the coarse-scale observations into a finer grid space, resulting in the preservation of the model's intrinsic resolution.

(Please insert Figure 12 here)

The impact of GRACE DA is also observed in water redistribution within the water storage components. Figure 13 shows the contributions of four different water storage components (SMS, GWS, SWE, and CNP) to TWS in different basins before (CABLE 0.05°, Fig. 13a) and after the application of GRACE DA (GRACE DA 0.05°, Fig. 13b). The contribution is calculated as a percent of the annual amplitude of the water storage component and the amplitude of the TWS. In CABLE 0.05° (Fig. 13a), the SMS is a major contributor to more than 90% of the TWS. The GWS contribution is only ~10 %. After applying GRACE DA (Fig. 13b), the contribution of the GWS is significantly increased. It dominates the entire water column in several basins (e.g., Indian Ocean, Lake Eyre, North West Plateau, South West Plateau). A similar finding is also seen in, e.g., Girotto et al. (2016), Tangdamrongsub et al. (2018), Li et al. (2019), who reported a clear impact of GRACE DA on deep storage components (e.g., GWS). The contributions of the SWE and CNP components are negligible across Australia, and the impact of GRACE DA on them is trivial. Similar changes to TWS contributions are also observed between CABLE 0.5° and GRACE DA 0.5° (not shown). It is noted that Fig. 12 and Fig. 13 only present the impact of GRACE DA on storage components and do not assess the accuracy of either version. The accuracy of the OL and DA models is quantified in Sect. 4.3.

(Please insert Figure 13 here)

4.3 Validation with in situ data

In situ data from three different ground networks (see Sect. 2.3.2) are used to validate the GWS, ET, and SSM estimates. Validation is conducted by quantifying the change in correlation values between simulations and observations when one model

is used in place of another. The validation period is between January 2003 and December 2012, consistent with the GRACE DA period. Figure 14 shows the validation of GWS estimates between GRACE DA and OL simulations (DA minus OL). A positive value indicates improvement, while a negative value represents degradation. A significance test is performed at the 0.05 level based on the Fisher Z-transform test for correlation coefficients (Zaitchick et al., 2008). The average change in
415 correlation value across all in situ data site are shown in Fig. 14d. Values that failed the significant test are excluded from the averaging.

(Please insert Figure 14 here)

We first analyze the impact of GRACE DA on the GWS estimates of CABLE 0.5° and CABLE 0.05° (Fig. 14a and 14b). A greater correlation improvement is observed when GRACE DA is applied to the 0.5° model, which increases the average
420 correlation value by 0.23 (Fig. 14d1). When GRACE DA is applied to the 0.05° model (Fig. 14b), the average correlation value improves by 0.12 (Fig. 14d6), ~50% less than in the 0.5° model.

When comparing the two OL runs (CABLE 0.5° vs. CABLE 0.05°), the GWS estimate from CABLE 0.05° has a higher correlation value by 0.12 (see Fig. 14d2). This analysis indicates that the lower correlation improvement seen between CABLE 0.05° and GRACE DA 0.05° is unlikely caused by the reduced impact of GRACE DA on the high-resolution model. Rather,
425 it is a result of CABLE 0.05° having better accuracy to start with. GRACE DA tends to provide the same information to both 0.5° and 0.05° models. Still, GRACE DA 0.05° exhibits the best correlation with in situ data, ~0.02 higher than GRACE DA 0.5° (Fig. 14c and Fig. 14d5). While GWS estimates from both CABLE 0.5° and CABLE 0.05° improve with GRACE DA, we find that CABLE 0.05° (OL) shows a higher correlation value than the GRACE DA 0.5° (DA) by 0.1 (see Fig. 14d3). This denotes that the improved model parameters are as important as the improved model state estimates (e.g., via DA).

430 SSM and ET estimates are validated against ground measurements from SASMAS and Ozenet, respectively. Correlation coefficients between the case study simulations and observation networks are summarized in Fig. 15. For SSM (Fig. 15a), CABLE 0.05° exhibits slightly improved correlation with observations (by ~0.6 %) than does CABLE 0.5°. The addition of GRACE DA also shows a small but positive impact on SSM estimates, improving correlation with observations by ~1 %. The small impact is attributed to limited GRACE sensitivity. GRACE is sensitive to the low-frequency variation (originated from
435 deeper stores) and cannot effectively capture SSM, which is dominated by a high-frequency signal (e.g., precipitation). As a result, GRACE DA is found to have a minor (or negative) impact on the top soil component in most GRACE DA studies (e.g., Li et al., 2012; Tian et al., 2017; Tangdamrongsub et al., 2020).

(Please insert Figure 15 here)

For ET (Fig. 15b), CABLE 0.05° exhibits improved correlation with observations (by ~5 %) than does CABLE 0.5°. The
440 inclusion of GRACE DA also slightly improves correlation values over the associated OL model versions. Greater improvement (by ~2%) is seen between CABLE 0.5° and GRACE DA 0.5° than between CABLE 0.05° and GRACE DA 0.05°. As with SSM, the small improvement of ET is likely attributable in part to small GRACE DA updates (caused by the

limited GRACE sensitivity to high-frequency surface fluxes). The SSM is a primary moisture source for ET, so a trivial change in SSM leads to a similarly small change in ET.

5 Conclusion

445

This study enhances the spatial resolution and timespan (> 30 years) of regional TWS estimates using the CABLE LSM, high-resolution land cover maps and forcing data, and GRACE DA application. By improving the model parameter and forcing data (without GRACE DA), the developed CABLE 0.05° model shows clear improvements in the accuracy of water balance component estimates (e.g., soil moisture, groundwater, evapotranspiration) compared with in situ and independent satellite

450 data. The 0.05° model also improves the spatial resolution by a factor of two to three over the 0.5° version. The extended timespan provides insightful information for long-term assessment of regional water resources and climate variability. The enhanced model parameterization is found to play a significant role in the improved TWS estimates. Incorporating GRACE DA into the model leads to further improvements of TWS component estimates. The positive impact of GRACE DA is found in the deep storage component (e.g., GWS), while the impact on the surface components and flux estimates (i.e., SSM and ET)

455 is trivial. Of the four case studies investigated here, the most accurate simulation uses CABLE 0.05° with GRACE DA.

The enhanced CABLE model resolution developed in this study relies on improved parameter and forcing data. The land surface physics remain unchanged. The workflow can be adopted for other CABLE repositories or different LSM with only slight modifications, e.g., number of soil or vegetation types. The CABLE 0.05° TWS estimates can be reproduced at locations outside the area studied here since high resolution forcing data and model parameters are available globally (or

460 near globally). Future development can consider extending the temporal record or further increasing the spatial resolution of TWS estimates. The timespan extension is feasible using reanalysis forcing data from the Modern-Era Retrospective Analysis for Research and Applications, Version 2 (MERRA-2; Gelaro et al., 2017), which would allow TWS simulations to be extended to the near present. Similarly, the TWS estimates could approach sub-kilometer scale grid spacing by using a number of high-resolution land parameter sets, e.g., a 250 m soil map (Hengl et al., 2017) and a 500 m LAI data (Myneni et

465 al., 2015).

Data availability

The model and data used in this study are publicly available and can be accessed as follows (last accessed: 6 May 2020):
- CABLE model: https://trac.nci.org.au/trac/cable
- The Harmonized World Soil Database version 1.2: http://www.fao.org/soils-portal/soil-survey/soil-maps-and-
470 databases/harmonized-world-soil-database-v12/en
- The global land cover climatology using MODIS data:
https://archive.usgs.gov/archive/sites/landcover.usgs.gov/global_climatology.html

- The Global Land Surface Satellite: http://www.glass.umd.edu
- The Princeton forcing data: https://hydrology.princeton.edu/data.pgf.php
475 - The Climate Hazards Group InfraRed Precipitation with Station data: https://chc.ucsb.edu/data/chirps
- GRACE GSFC mascon: https://earth.gsfc.nasa.gov/geo/data/grace-mascons
- The ESA-CCI: https://www.esa-soilmoisture-cci.org
- The Global Land Evaporation Amsterdam Model: https://www.gleam.eu
- In situ soil moisture: http://www.eng.newcastle.edu.au/sasmas/SASMAS/sasdata.html,
480 https://ismn.geo.tuwien.ac.at/en
- In situ groundwater: http://www.bom.gov.au/water/groundwater/explorer/map.shtml
- In situ evapotranspiration: https://fluxnet.fluxdata.org/data/fluxnet2015-dataset

Author contribution

NT: Conceptualization, formal analysis, software, validation, visualization, and writing original paper. MJ: supervision,
485 funding acquisition. PS: editing paper.

Competing interests

The authors declare that they have no conflict of interest.

Acknowledgments

This work was supported by the NASA Earth Science Division in support of the National Climate Assessment. NT thanks
490 Mark Decker for CABLE-SSGW model development.

References

Alkama, R., Decharme, B., Douville, H., Becker, M., Cazenave, A., Sheffield, J., Voldoire, A., Tyteca, S. and Le Moigne, P.:
Global Evaluation of the ISBA-TRIP Continental Hydrological System. Part I: Comparison to GRACE Terrestrial Water
Storage Estimates and In Situ River Discharges, J. Hydrometeor., 11(3), 583–600, doi:10.1175/2010JHM1211.1, 2010.

495 Beamer, J. P., Hill, D. F., Arendt, A. and Liston, G. E.: High-resolution modeling of coastal freshwater discharge and glacier
mass balance in the Gulf of Alaska watershed, Water Resour. Res., 52(5), 3888–3909, doi:10.1002/2015WR018457, 2016.

Bi, D., Dix, M., Marsland, S., O'Farrell, S., Rashid, H., Uotila, P., Hirst, T., Kowalczyk, E., Golebiewski, M., Sullivan, A.,
Yan, H., Hannah, N., Franklin, C., Sun, Z., Vohralik, P., Watterson, I., Zhou, X., Fiedler, R., Collier, M., Ma, Y., Noonan, J.,

Stevens, L., Uhe, P., Zhu, H., Griffies, S., Hill, R., Harris, C. and Puri, K.: The ACCESS Coupled Model: Description, Control
500   Climate and Evaluation, Aust. Meteorol. Oceanogr. J., 63, 41–64, doi:https://doi.org/10.22499/2.6301.004, 2013.

Bierkens Marc F. P.: Global hydrology 2015: State, trends, and directions, Water Resour. Res., 51(7), 4923–4947,
doi:10.1002/2015WR017173, 2015.

Bierkens, M. F. P., Bell, V. A., Burek, P., Chaney, N., Condon, L. E., David, C. H., Roo, A. de, Döll, P., Drost, N., Famiglietti,
J. S., Flörke, M., Gochis, D. J., Houser, P., Hut, R., Keune, J., Kollet, S., Maxwell, R. M., Reager, J. T., Samaniego, L.,
505   Sudicky, E., Sutanudjaja, E. H., Giesen, N. van de, Winsemius, H. and Wood, E. F.: Hyper-resolution global hydrological
modelling: what is next?, Hydrol. Process., 29(2), 310–320, doi:10.1002/hyp.10391, 2015.

Bond, N. R., Lake, P. S. and Arthington, A. H.: The impacts of drought on freshwater ecosystems: an Australian perspective,
Hydrobiologia, 600(1), 3–16, doi:10.1007/s10750-008-9326-z, 2008.

Broxton, P. D., Zeng, X., Sulla-Menashe, D. and Troch, P. A.: A Global Land Cover Climatology Using MODIS Data, J. Appl.
510   Meteorol. Clim., 53(6), 1593–1605, doi:10.1175/JAMC-D-13-0270.1, 2014.

Castellazzi, P., Martel, R., Galloway, D. L., Longuevergne, L. and Rivera, A.: Assessing Groundwater Depletion and
Dynamics Using GRACE and InSAR: Potential and Limitations, Groundwater, 54(6), 768–780, doi:10.1111/gwat.12453,
2016.

Crow Wade T., Berg Aaron A., Cosh Michael H., Loew Alexander, Mohanty Binayak P., Panciera Rocco, Rosnay Patricia,
515   Ryu Dongryeol and Walker Jeffrey P.: Upscaling sparse ground-based soil moisture observations for the validation of coarse-
resolution satellite soil moisture products, Rev. Geophys., 50(2), doi:10.1029/2011RG000372, 2012.

Decker, M.: Development and evaluation of a new soil moisture and runoff parameterization for the CABLE LSM including
subgrid-scale processes, J. Adv. Model. Earth Syst., 7(4), 1788–1809, doi:10.1002/2015MS000507, 2015.

Delworth, T. L. and Manabe, S.: The Influence of Potential Evaporation on the Variabilities of Simulated Soil Wetness and
520   Climate, J. Climate, 1(5), 523–547, doi:10.1175/1520-0442(1988)001<0523:TIOPEO>2.0.CO;2, 1988.

Dong, B., Lenters, J. D., Hu, Q., Kucharik, C. J., Wang, T., Soylu, M. E. and Mykleby, P. M.: Decadal-scale changes in the
seasonal surface water balance of the central U.S. from 1984-2007, J. Hydrometeor., doi:10.1175/JHM-D-19-0050.1, 2020.

Dong, J. and Crow, W. T.: The Added Value of Assimilating Remotely Sensed Soil Moisture for Estimating Summertime Soil
Moisture-Air Temperature Coupling Strength, Water Resources Research, 54(9), 6072–6084, doi:10.1029/2018WR022619,
525   2018.

Dorigo, W., Wagner, W., Albergel, C., Albrecht, F., Balsamo, G., Brocca, L., Chung, D., Ertl, M., Forkel, M., Gruber, A.,
Haas, E., Hamer, P. D., Hirschi, M., Ikonen, J., de Jeu, R., Kidd, R., Lahoz, W., Liu, Y. Y., Miralles, D., Mistelbauer, T.,
Nicolai-Shaw, N., Parinussa, R., Pratola, C., Reimer, C., van der Schalie, R., Seneviratne, S. I., Smolander, T. and Lecomte,

P.: ESA CCI Soil Moisture for improved Earth system understanding: State-of-the art and future directions, Remote Sens
530   Environ., 203, 185–215, doi:10.1016/j.rse.2017.07.001, 2017.

Dorigo, W. A., Xaver, A., Vreugdenhil, M., Gruber, A., Hegyiová, A., Sanchis-Dufau, A. D., Zamojski, D., Cordes, C.,
Wagner, W. and Drusch, M.: Global Automated Quality Control of In Situ Soil Moisture Data from the International Soil
Moisture Network, Vadose Zone J., 12(3), doi:10.2136/vzj2012.0097, 2013.

Entekhabi, D., Njoku, E. G., O'Neill, P. E., Kellogg, K. H., Crow, W. T., Edelstein, W. N., Entin, J. K., Goodman, S. D.,
535   Jackson, T. J., Johnson, J., Kimball, J., Piepmeier, J. R., Koster, R. D., Martin, N., McDonald, K. C., Moghaddam, M., Moran,
S., Reichle, R., Shi, J. C., Spencer, M. W., Thurman, S. W., Tsang, L. and Zyl, J. V.: The Soil Moisture Active Passive (SMAP)
Mission, Proc. IEEE, 98(5), 704–716, doi:10.1109/JPROC.2010.2043918, 2010a.

Entekhabi, D., Reichle, R. H., Koster, R. D. and Crow, W. T.: Performance Metrics for Soil Moisture Retrievals and
Application Requirements, J. Hydrometeor., 11(3), 832–840, doi:10.1175/2010JHM1223.1, 2010b.

540   Fischer, E. M., Seneviratne, S. I., Vidale, P. L., Lüthi, D. and Schär, C.: Soil Moisture–Atmosphere Interactions during the
2003 European Summer Heat Wave, J. Climate, 20(20), 5081–5099, doi:10.1175/JCLI4288.1, 2007.

Forman, B. A., Reichle, R. H. and Rodell, M.: Assimilation of terrestrial water storage from GRACE in a snow-dominated
basin, Water Resour. Res., 48(1), W01507, doi:10.1029/2011WR011239, 2012.

Friedl, M. A., McIver, D. K., Hodges, J. C. F., Zhang, X. Y., Muchoney, D., Strahler, A. H., Woodcock, C. E., Gopal, S.,
545   Schneider, A., Cooper, A., Baccini, A., Gao, F. and Schaaf, C.: Global land cover mapping from MODIS: algorithms and early
results, Remote Sens Environ., 83(1), 287–302, doi:10.1016/S0034-4257(02)00078-0, 2002.

Funk, C., Peterson, P., Landsfeld, M., Pedreros, D., Verdin, J., Shukla, S., Husak, G., Rowland, J., Harrison, L., Hoell, A. and
Michaelsen, J.: The climate hazards infrared precipitation with stations—a new environmental record for monitoring extremes,
Sci. Data, 2(1), 1–21, doi:10.1038/sdata.2015.66, 2015.

550   Gelaro, R., McCarty, W., Suárez, M. J., Todling, R., Molod, A., Takacs, L., Randles, C. A., Darmenov, A., Bosilovich, M. G.,
Reichle, R., Wargan, K., Coy, L., Cullather, R., Draper, C., Akella, S., Buchard, V., Conaty, A., da Silva, A. M., Gu, W., Kim,
G.-K., Koster, R., Lucchesi, R., Merkova, D., Nielsen, J. E., Partyka, G., Pawson, S., Putman, W., Rienecker, M., Schubert, S.
D., Sienkiewicz, M. and Zhao, B.: The Modern-Era Retrospective Analysis for Research and Applications, Version 2
(MERRA-2), J. Climate, 30(14), 5419–5454, doi:10.1175/JCLI-D-16-0758.1, 2017.

555   Girotto, M., De Lannoy, G. J. M., Reichle, R. H. and Rodell, M.: Assimilation of gridded terrestrial water storage observations
from GRACE into a land surface model, Water Resour. Res., 52(5), 4164–4183, doi:10.1002/2015WR018417, 2016.

Girotto, M., De Lannoy, G. J. M., Reichle, R. H., Rodell, M., Draper, C., Bhanja, S. N. and Mukherjee, A.: Benefits and pitfalls of GRACE data assimilation: A case study of terrestrial water storage depletion in India, Geophys. Res. Lett., 44(9), 4107–4115, doi:10.1002/2017GL072994, 2017.

560 Gruber, A., Scanlon, T., van der Schalie, R., Wagner, W. and Dorigo, W.: Evolution of the ESA CCI Soil Moisture climate data records and their underlying merging methodology, Earth Syst. Sci. Data, 11(2), 717–739, doi:https://doi.org/10.5194/essd-11-717-2019, 2019.

Haverd, V., Smith, B., Nieradzik, L., Briggs, P. R., Woodgate, W., Trudinger, C. M., Canadell, J. G. and Cuntz, M.: A new version of the CABLE land surface model (Subversion revision r4601) incorporating land use and land cover change, woody
565 vegetation demography, and a novel optimisation-based approach to plant coordination of photosynthesis, Geosci. Model Dev., 11(7), 2995–3026, doi:https://doi.org/10.5194/gmd-11-2995-2018, 2018.

Hengl, T., Jesus, J. M. de, Heuvelink, G. B. M., Gonzalez, M. R., Kilibarda, M., Blagotić, A., Shangguan, W., Wright, M. N., Geng, X., Bauer-Marschallinger, B., Guevara, M. A., Vargas, R., MacMillan, R. A., Batjes, N. H., Leenaars, J. G. B., Ribeiro, E., Wheeler, I., Mantel, S. and Kempen, B.: SoilGrids250m: Global gridded soil information based on machine learning, PLOS
570 ONE, 12(2), e0169748, doi:10.1371/journal.pone.0169748, 2017.

Hirschi, M., Seneviratne, S. I., Hagemann, S. and Schär, C.: Analysis of seasonal terrestrial water storage variations in regional climate simulations over Europe, J. Geophys. Res., 112(D22), D22109, doi:10.1029/2006JD008338, 2007.

IPCC, 2007. Climate Change: The Physical Science Basis. Geneva: Intergovernmental Panel on Climate Change.

Jung, H. C., Getirana, A., Arsenault, K. R., Kumar, S. and Maigary, I.: Improving surface soil moisture estimates in West
575 Africa through GRACE data assimilation, J. Hydrol., 575, 192–201, doi:10.1016/j.jhydrol.2019.05.042, 2019.

Ke, Y., Leung, L. R., Huang, M., Coleman, A. M., Li, H. and Wigmosta, M. S.: Development of high resolution land surface parameters for the Community Land Model, Geosci. Model Dev., 5(6), 1341–1362, doi:https://doi.org/10.5194/gmd-5-1341-2012, 2012.

Khaki, M., Ait-El-Fquih, B., Hoteit, I., Forootan, E., Awange, J. and Kuhn, M.: A two-update ensemble Kalman filter for land
580 hydrological data assimilation with an uncertain constraint, J. Hydrol., 555, 447–462, doi:10.1016/j.jhydrol.2017.10.032, 2017.

Klees, R., Liu, X., Wittwer, T., Gunter, B. C., Revtova, E. A., Tenzer, R., Ditmar, P., Winsemius, H. C. and Savenije, H. H. G.: A Comparison of Global and Regional GRACE Models for Land Hydrology, Surv. Geophys., 29(4–5), 335–359, doi:10.1007/s10712-008-9049-8, 2008.

Kollet, S. J. and Maxwell, R. M.: Capturing the influence of groundwater dynamics on land surface processes using an
585 integrated, distributed watershed model, Water Resour. Res., 44(2), doi:10.1029/2007WR006004, 2008.

Koster, R. D., Suarez, M. J., Ducharne, A., Stieglitz, M. and Kumar, P.: A catchment-based approach to modeling land surface processes in a general circulation model: 1. Model structure, J. Geophys. Res., 105(D20), 24809–24822, doi:10.1029/2000JD900327, 2000.

Koster, R. D. and Suarez, M. J.: Soil Moisture Memory in Climate Models, J. Hydrometeor., 2(6), 558–570, doi:10.1175/1525-
590   7541(2001)002<0558:SMMICM>2.0.CO;2, 2001.

Koster, R. D., Sud, Y. C., Guo, Z., Dirmeyer, P. A., Bonan, G., Oleson, K. W., Chan, E., Verseghy, D., Cox, P., Davies, H., Kowalczyk, E., Gordon, C. T., Kanae, S., Lawrence, D., Liu, P., Mocko, D., Lu, C.-H., Mitchell, K., Malyshev, S., McAvaney, B., Oki, T., Yamada, T., Pitman, A., Taylor, C. M., Vasic, R. and Xue, Y.: GLACE: The Global Land–Atmosphere Coupling Experiment. Part I: Overview, J. Hydrometeor., 7(4), 590–610, doi:10.1175/JHM510.1, 2006.

595   Kowalczyk, E. A., Wang, Y. P., Law, R. M., Davies, H. L., McGregor, J. L., Abramowitz, G. S.: The CSIRO Atmosphere Biosphere Land Exchange (CABLE) model for use in climate models and as an offline model. Aspendale, Vic., CSIRO Marine and Atmospheric Research. https://doi.org/10.4225/08/58615c6a9a51d, 2006.

Kowalczyk, E., Stevens, L., Law, R., Dix, M., Wang, Y., Harman, I., Haynes, K., Srbinovsky, J., Pak, B., and Ziehn, T.: The land surface model component of ACCESS: description and impact on the simulated surface climatology, Aust. Meteorol.
600   Oceanogr. J., 63, 65–82, 2013.

Kumar, S. V., M. Mocko, D., Wang, S., Peters-Lidard, C. D. and Borak, J.: Assimilation of Remotely Sensed Leaf Area Index into the Noah-MP Land Surface Model: Impacts on Water and Carbon Fluxes and States over the Continental United States, J. Hydrometeor., 20(7), 1359–1377, doi:10.1175/JHM-D-18-0237.1, 2019.

Kumar, S. V., Zaitchik, B. F., Peters-Lidard, C. D., Rodell, M., Reichle, R., Li, B., Jasinski, M., Mocko, D., Getirana, A., De
605   Lannoy, G., Cosh, M. H., Hain, C. R., Anderson, M., Arsenault, K. R., Xia, Y. and Ek, M.: Assimilation of Gridded GRACE Terrestrial Water Storage Estimates in the North American Land Data Assimilation System, J. Hydrometeor., 17(7), 1951–1972, doi:10.1175/JHM-D-15-0157.1, 2016.

Li, B., Rodell, M., Kumar, S., Beaudoing, H. K., Getirana, A., Zaitchik, B. F., Goncalves, L. G. de, Cossetin, C., Bhanja, S., Mukherjee, A., Tian, S., Tangdamrongsub, N., Long, D., Nanteza, J., Lee, J., Policelli, F., Goni, I. B., Daira, D., Bila, M.,
610   Lannoy, G. de, Mocko, D., Steele-Dunne, S. C., Save, H. and Bettadpur, S.: Global GRACE Data Assimilation for Groundwater and Drought Monitoring: Advances and Challenges, Water Resour. Res., 55(9), 7564–7586, doi:10.1029/2018WR024618, 2019.

Li, B., Rodell, M., Zaitchik, B. F., Reichle, R. H., Koster, R. D. and van Dam, T. M.: Assimilation of GRACE terrestrial water storage into a land surface model: Evaluation and potential value for drought monitoring in western and central Europe, J.
615   Hydrol., 446–447, 103–115, doi:10.1016/j.jhydrol.2012.04.035, 2012.

Luthcke, S. B., Arendt, A. A., Rowlands, D. D., McCarthy, J. J. and Larsen, C. F.: Recent glacier mass changes in the Gulf of Alaska region from GRACE mascon solutions, J. Glaciol., 54(188), 767–777, doi:10.3189/002214308787779933, 2008.

Luthcke, S. B., Sabaka, T. J., Loomis, B. D., Arendt, A. A., McCarthy, J. J. and Camp, J.: Antarctica, Greenland and Gulf of Alaska land-ice evolution from an iterated GRACE global mascon solution, J. Glaciol., 59(216), 613–631, doi:10.3189/2013JoG12J147, 2013.

Martens, B., Miralles, D. G., Lievens, H., Schalie, R. van der, Jeu, R. A. M. de, Fernández-Prieto, D., Beck, H. E., Dorigo, W. A. and Verhoest, N. E. C.: GLEAM v3: satellite-based land evaporation and root-zone soil moisture, Geosci. Model Dev., 10(5), 1903–1925, doi:https://doi.org/10.5194/gmd-10-1903-2017, 2017.

McNally, A., Arsenault, K., Kumar, S., Shukla, S., Peterson, P., Wang, S., Funk, C., Peters-Lidard, C. D. and Verdin, J. P.: A land data assimilation system for sub-Saharan Africa food and water security applications, Sci. Data, 4, 170012, doi:10.1038/sdata.2017.12, 2017.

Mouyen, M., Longuevergne, L., Steer, P., Crave, A., Lemoine, J.-M., Save, H. and Robin, C.: Assessing modern river sediment discharge to the ocean using satellite gravimetry, Nat. Commun., 9(1), 3384, doi:10.1038/s41467-018-05921-y, 2018.

Munier, S., Becker, M., Maisongrande, P., Cazenave, A.: Using GRACE to detect groundwater storage variations: The cases of Canning Basin and Guarni aquifer system, International Water Technology Journal 2, 2–13, 2012.

Murphy, B. F. and Timbal, B.: A review of recent climate variability and climate change in southeastern Australia, Int. J. Climatol., 28(7), 859–879, doi:10.1002/joc.1627, 2008.

Müller Schmied, H.: Evaluation, Modification and Application of a Global Hydrological Model. Ph.D. Thesis, Institute of Physical Geography, Goethe University Frankfurt, Frankfurt am Main, Germany, 2017.

Myneni, R., Y. Knyazikhin, T. Park, 2015. MCD15A2H MODIS/Terra+Aqua Leaf Area Index/FPAR 8-day L4 Global 500m SIN Grid V006. NASA EOSDIS Land Processes DAAC, https://doi.org/10.5067/MODIS/MCD15A2H.006 (Last access: 28 February 2020).

Nachtergaele, F., van Velthuizen, H., Verelst, L., Batjes, N., Dijkshoorn, K., van Engelen, V., Fischer, G., Jones, A., Montanarella, L., Petri, M.: Harmonized World Soil Database, Version 1.2, Wageningen, Rome, Italy, 2009.

National Academies of Sciences, Engineering, and Medicine. 2018.Thriving on Our Changing Planet: A Decadal Strategy for Earth Observation from Space. Washington, DC: The National Academies Press. https://doi.org.10.17226/24938.

Nie, W., Zaitchik, B. F., Rodell, M., Kumar, S. V., Arsenault, K. R., Li, B. and Getirana, A.: Assimilating GRACE Into a Land Surface Model in the Presence of an Irrigation-Induced Groundwater Trend, Water Resour. Res., 55(12), 11274–11294, doi:10.1029/2019WR025363, 2019.

645   Oleson, W., Lawrence, M., Bonan, B., Flanner, G., Kluzek, E., Lawrence, J., Levis, S., Swenson, C., Thornton, E., Dai, A.,
       Decker, M., Dickinson, R., Feddema, J., Heald, L., Hoffman, F., Lamarque, J.-F., Mahowald, N., Niu, G.-Y., Qian, T.,
       Randerson, J., Running, S., Sakaguchi, K., Slater, A., Stockli, R., Wang, A., Yang, Z.-L., Xiaodong, Z., Xubin, Z.: Technical
       Description of version 4.0 of the Community Land Model (CLM) (No. NCAR/TN-478+STR). University Corporation for
       Atmospheric Research. doi:10.5065/D6FB50WZ, 2010.

650   Pastorello, G.Z., Papale, D., Chu, H., Trotta, C., Agarwal, D.A., Canfora, E., Baldocchi, D.D., Torn, M.S.: A new data set to
       keep a sharper eye on land-air exchanges, Eos 98, http://dx.doi.org/10.1029/2017EO071597, 2017.

       Peltier, W. R., Argus, D. F., Drummond, R.: Space geodesy constrains ice-age terminal deglaciation: The global ICE-6G C
       (VM5a) model, J. Geophys. Res. Solid Earth, 120, 450-487, doi:10.1002/2014JB011176, 2015.

       Pitman, A. J.: The evolution of, and revolution in, land surface schemes designed for climate models, Int. J. Climatol., 23,
655   479–510, https://doi.org/10.1002/joc.893, 2003.

       Quiring, S. M.: Developing Objective Operational Definitions for Monitoring Drought, J. Appl. Meteor. Climatol. 48, 1217–
       1229, https://doi.org/10.1175/2009JAMC2088.1, 2009.

       Rasmussen, R., Ikeda, K., Liu, C., Gochis, D., Clark, M., Dai, A., Gutmann, E., Dudhia, J., Chen, F., Barlage, M., Yates, D.
       and Zhang, G.: Climate Change Impacts on the Water Balance of the Colorado Headwaters: High-Resolution Regional Climate
660   Model Simulations, J. Hydrometeor., 15(3), 1091–1116, doi:10.1175/JHM-D-13-0118.1, 2014.

       Raupach,M. R., Briggs, P. R., Haverd, V., King, E. A., Paget, M., & Trudinger, C. M.: Australian Water Availability Project
       (AWAP) CSIRO Marine and Atmospheric Research Component: Final Report for Phase 3. Canberra, Australia: CSIRO
       Marine   and   Atmospheric   Research,   2008,   Available   online   at:
       http://www.csiro.au/awap/doc/AWAP3.FinalReport.20080601.V07.pdf (Last access: 16 Feb 2020).

665   Reichle, R. H.: Data assimilation methods in the Earth sciences, Adv. Water Resour., 31(11), 1411–1418,
       doi:10.1016/j.advwatres.2008.01.001, 2008.

       Reichle, R. H., McLaughlin, D. B. and Entekhabi, D.: Hydrologic Data Assimilation with the Ensemble Kalman Filter, Mon.
       Wea. Rev., 130(1), 103–114, doi:10.1175/1520-0493(2002)130<0103:HDAWTE>2.0.CO;2, 2002.

       Richey, A. S., Thomas, B. F., Lo, M. -H., Reager, J. T., Famiglietti, J. S., Voss, K., Swenson, S., Rodell, M.: Quantifying
670   renewable groundwater stress with GRACE, Water Resour. Res., 51(7), 5217–5238, doi:10.1002/2015WR017349, 2015.

       Rodell, M., Famiglietti, J. S., Wiese, D. N., Reager, J. T., Beaudoing, H. K., Landerer, F. W. and Lo, M.-H.: Emerging trends
       in global freshwater availability, Nature, 557(7707), 651–659, doi:10.1038/s41586-018-0123-1, 2018.

Rodell, M., Houser, P. R., Jambor, U., Gottschalck, J., Mitchell, K., Meng, C.-J., Arsenault, K., Cosgrove, B., Radakovich, J., Bosilovich, M., Entin*, J. K., Walker, J. P., Lohmann, D. and Toll, D.: The Global Land Data Assimilation System, Bull.

675 Amer. Meteor. Soc., 85(3), 381–394, doi:10.1175/BAMS-85-3-381, 2004.

Rowlands, D. D., Luthcke, S. B., McCarthy, J. J., Klosko, S. M., Chinn, D. S., Lemoine, F. G., Boy, J.-P. and Sabaka, T. J.: Global mass flux solutions from GRACE: A comparison of parameter estimation strategies—Mass concentrations versus Stokes coefficients, J. Geophys. Res. Solid Earth, 115(B1), doi:10.1029/2009JB006546, 2010.

Rüdiger, C., Hancock, G., Hemakumara, H. M., Jacobs, B., Kalma, J. D., Martinez, C., Thyer, M., Walker, J. P., Wells, T. and

680 Willgoose, G. R.: Goulburn River experimental catchment data set, Water Resour. Res., 43(10), W10403, doi:10.1029/2006WR005837, 2007.

Schumacher, M., Forootan, E., van Dijk, A. I. J. M., Müller Schmied, H., Crosbie, R. S., Kusche, J. and Döll, P.: Improving drought simulations within the Murray-Darling Basin by combined calibration/assimilation of GRACE data into the WaterGAP Global Hydrology Model, Remote Sens Environ., 204, 212–228, doi:10.1016/j.rse.2017.10.029, 2018.

685 Seneviratne, S. I., Corti, T., Davin, E. L., Hirschi, M., Jaeger, E. B., Lehner, I., Orlowsky, B. and Teuling, A. J.: Investigating soil moisture–climate interactions in a changing climate: A review, Earth-Sci. Rev., 99(3), 125–161, doi:10.1016/j.earscirev.2010.02.004, 2010.

Sheffield, J., Goteti, G. and Wood, E. F.: Development of a 50-Year High-Resolution Global Dataset of Meteorological Forcings for Land Surface Modeling, J. Climate, 19(13), 3088–3111, doi:10.1175/JCLI3790.1, 2006.

690 Shokri, A., Walker, J. P., Dijk, A. I. J. M. van and Pauwels, V. R. N.: On the Use of Adaptive Ensemble Kalman Filtering to Mitigate Error Misspecifications in GRACE Data Assimilation, Water Resour. Res., 55(9), 7622–7637, doi:10.1029/2018WR024670, 2019.

Singh, R. S., Reager, J. T., Miller, N. L. and Famiglietti, J. S.: Toward hyper-resolution land-surface modeling: The effects of fine-scale topography and soil texture on CLM4.0 simulations over the Southwestern U.S., Water Resour. Res., 51(4), 2648–

695 2667, doi:10.1002/2014WR015686, 2015.

Sutanudjaja, E. H., van Beek, R., Wanders, N., Wada, Y., Bosmans, J. H. C., Drost, N., van der Ent, R. J., de Graaf, I. E. M., Hoch, J. M., de Jong, K., Karssenberg, D., López López, P., Peßenteiner, S., Schmitz, O., Straatsma, M. W., Vannametee, E., Wisser, D. and Bierkens, M. F. P.: PCR-GLOBWB 2: a 5 arcmin global hydrological and water resources model, Geosci. Model Dev., 11(6), 2429–2453, doi:10.5194/gmd-11-2429-2018, 2018.

700 Tangdamrongsub, N., Han, S.-C., Jasinski, M. F. and Šprlák, M.: Quantifying water storage change and land subsidence induced by reservoir impoundment using GRACE, Landsat, and GPS data, Remote Sens Environ., 233, 111385, doi:10.1016/j.rse.2019.111385, 2019.

Tangdamrongsub, N., Han, S.-C., Tian, S., Müller Schmied, H., Sutanudjaja, E. H., Ran, J. and Feng, W.: Evaluation of Groundwater Storage Variations Estimated from GRACE Data Assimilation and State-of-the-Art Land Surface Models in Australia and the North China Plain, Remote Sens., 10(3), 483, doi:10.3390/rs10030483, 2018.

Tangdamrongsub, N., Han, S.-C., Yeo, I.-Y., Dong, J., Steele-Dunne, S. C., Willgoose, G. and Walker, J. P.: Multivariate data assimilation of GRACE, SMOS, SMAP measurements for improved regional soil moisture and groundwater storage estimates, Adv. Water Resour., 135, 103477, doi:10.1016/j.advwatres.2019.103477, 2020.

Tangdamrongsub, N., Steele-Dunne, S. C., Gunter, B. C., Ditmar, P. G. and Weerts, A. H.: Data assimilation of GRACE terrestrial water storage estimates into a regional hydrological model of the Rhine River basin, Hydrol. Earth Syst. Sci., 19(4), 2079–2100, doi:10.5194/hess-19-2079-2015, 2015.

Tangdamrongsub, N., Steele-Dunne, S. C., Gunter, B. C., Ditmar, P. G., Sutanudjaja, E. H., Sun, Y., Xia, T. and Wang, Z.: Improving estimates of water resources in a semi-arid region by assimilating GRACE data into the PCR-GLOBWB hydrological model, Hydrol. Earth Syst. Sci., 21(4), 2053–2074, doi:https://doi.org/10.5194/hess-21-2053-2017, 2017.

Tapley, B. D., Bettadpur, S., Ries, J. C., Thompson, P. F. and Watkins, M. M.: GRACE Measurements of Mass Variability in the Earth System, Science, 305(5683), 503–505, doi:10.1126/science.1099192, 2004.

Tapley, B. D., Watkins, M. M., Flechtner, F., Reigber, C., Bettadpur, S., Rodell, M., Sasgen, I., Famiglietti, J. S., Landerer, F. W., Chambers, D. P., Reager, J. T., Gardner, A. S., Save, H., Ivins, E. R., Swenson, S. C., Boening, C., Dahle, C., Wiese, D. N., Dobslaw, H., Tamisiea, M. E. and Velicogna, I.: Contributions of GRACE to understanding climate change, Nat. Clim. Change, 9(5), 358, doi:10.1038/s41558-019-0456-2, 2019.

Tian, S., Tregoning, P., Renzullo, L. J., Dijk, A. I. J. M. van, Walker, J. P., Pauwels, V. R. N. and Allgeyer, S.: Improved water balance component estimates through joint assimilation of GRACE water storage and SMOS soil moisture retrievals, Water Resour. Res., 53(3), 1820–1840, doi:10.1002/2016WR019641, 2017.

Tscherning, C. C., and Rapp, R. H.: Closed covariance expressions for gravity anomalies, geoid undulations, and deflections of the vertical implied by anomaly degree variance models. Report 208, Dep. of Geod. Sci. and Surv., Ohio State Univ., Columbus, 1974.

Ukkola, A. M., Pitman, A. J., Decker, M., De Kauwe, M. G., Abramowitz, G., Kala, J. and Wang, Y.-P.: Modelling evapotranspiration during precipitation deficits: identifying critical processes in a land surface model, Hydrol. Earth Syst. Sci., 20(6), 2403–2419, doi:10.5194/hess-20-2403-2016, 2016.

van Dijk, A.: Landscape Model (version 0.5), AWRA Technical Report 3. WIRADA/CSIRO Water for a Healthy Country Flagship, Canberra, 2010, Available online at: http://www.clw.csiro.au/publications/waterforahealthycountry/2010/wfhc-aus-water-resources-assessment-system.pdf (Last access: 16 Feb 2020).

van Dijk, A. I. J. M., Beck, H. E., Crosbie, R. S., de Jeu, R. A. M., Liu, Y. Y., Podger, G. M., Timbal, B. and Viney, N. R.: The Millennium Drought in southeast Australia (2001–2009): Natural and human causes and implications for water resources, ecosystems, economy, and society, Water Resour. Res., 49(2), 1040–1057, doi:10.1002/wrcr.20123, 2013.

van Dijk, A. I. J. M., Peña-Arancibia, J. L., Wood, E. F., Sheffield, J. and Beck, H. E.: Global analysis of seasonal streamflow predictability using an ensemble prediction system and observations from 6192 small catchments worldwide, Water Resour. Res., 49(5), 2729–2746, doi:10.1002/wrcr.20251, 2013.

Dijk, A. I. J. M. van, Renzullo, L. J. and Rodell, M.: Use of Gravity Recovery and Climate Experiment terrestrial water storage retrievals to evaluate model estimates by the Australian water resources assessment system, Water Resour. Res., 47(11), doi:10.1029/2011WR010714, 2011.

Wang, Y. P., Kowalczyk, E., Leuning, R., Abramowitz, G., Raupach, M. R., Pak, B., van Gorsel, E. and Luhar, A.: Diagnosing errors in a land surface model (CABLE) in the time and frequency domains, J. Geophys. Res., 116(G1), G01034, doi:10.1029/2010JG001385, 2011.

Wilson, K., Goldstein, A., Falge, E., Aubinet, M., Baldocchi, D., Berbigier, P., Bernhofer, C., Ceulemans, R., Dolman, H., Field, C., Grelle, A., Ibrom, A., Law, B. E., Kowalski, A., Meyers, T., Moncrieff, J., Monson, R., Oechel, W., Tenhunen, J., Valentini, R. and Verma, S.: Energy balance closure at FLUXNET sites, Agric. For. Meteorol., 113(1), 223–243, doi:10.1016/S0168-1923(02)00109-0, 2002.

Wood, E. F., Roundy, J. K., Troy, T. J., Beek, L. P. H. van, Bierkens, M. F. P., Blyth, E., Roo, A. de, Döll, P., Ek, M., Famiglietti, J., Gochis, D., Giesen, N. van de, Houser, P., Jaffé, P. R., Kollet, S., Lehner, B., Lettenmaier, D. P., Peters-Lidard, C., Sivapalan, M., Sheffield, J., Wade, A. and Whitehead, P.: Hyperresolution global land surface modeling: Meeting a grand challenge for monitoring Earth's terrestrial water, Water Resour. Res., 47(5), doi:10.1029/2010WR010090, 2011.

Xiao, Z., Liang, S., Wang, J., Chen, P., Yin, X., Zhang, L. and Song, J.: Use of General Regression Neural Networks for Generating the GLASS Leaf Area Index Product From Time-Series MODIS Surface Reflectance, IEEE Trans. Geosci. Remote Sens., 52(1), 209–223, doi:10.1109/TGRS.2013.2237780, 2014.

Xie, Z., Huete, A., Restrepo-Coupe, N., Ma, X., Devadas, R. and Caprarelli, G.: Spatial partitioning and temporal evolution of Australia's total water storage under extreme hydroclimatic impacts, Remote Sens Environ., 183, 43–52, doi:10.1016/j.rse.2016.05.017, 2016.

Yuan, H., Dai, Y., Xiao, Z., Ji, D. and Shangguan, W.: Reprocessing the MODIS Leaf Area Index products for land surface and climate modelling, Remote Sens Environ., 115(5), 1171–1187, doi:10.1016/j.rse.2011.01.001, 2011.

Zaitchik, B. F., Rodell, M. and Reichle, R. H.: Assimilation of GRACE Terrestrial Water Storage Data into a Land Surface Model: Results for the Mississippi River Basin, J. Hydrometeor., 9(3), 535–548, doi:10.1175/2007JHM951.1, 2008.

Zobler, L. 1999. Global Soil Types, 1-Degree Grid (Zobler). ORNL DAAC, Oak Ridge, Tennessee, USA. https://doi.org/10.3334/ORNLDAAC/418.

765

Table 1: Relevant studies related to the development of the land surface and hydrology models (with the inclusion of GRACE DA applications) to estimate TWS in Australia.

Model	Spatial resolution	Timespan	GRACE DA approach	References
WaterGAP Global Hydrology Model (WGHM)	0.5°	2003 – 2010	EnKF	Müller Schmied (2017); Schumacher et al. (2018)
The World-Wide Water (W3)	0.5°	2002 – 2013	EnKF	van Dijk et al. (2013b); Tian et al. (2017)
World-Wide Water Resources Assessment (W3RA)	0.5°	2002 – 2013	Various	van Dijk (2010); Khaki et al. (2017)
PCRaster Global Water Balance (PCR-GLOBWB)	0.5°	2003 – 2014	EnKS 3D	Sutanudjaja et al. (2018); Tangdamrongsub et al. (2018)
NASA's Catchment land surface model (CLSM)	0.25°	2003 – 2012	EnKS	Koster et al. (2000); Li et al. (2019)
The Australian Water Resources Assessment - Landscape Model (AWRA-L)	0.05°	2000 – 2018	Adaptive EnKF	van Dijk (2010); Shokri et al. (2019)
The Community Atmosphere Biosphere Land Exchange (CABLE) 0.05°	0.05°	1980 – 2012	EnKS 3D	This study

Table 2: Characteristics of the land cover parameters, meteorological forcing, and remote sensing data used in the development
770   of CABLE 0.05°.

	Products	Grid size	Time interval	References
Meteorological Forcing data	Princeton forcing data version 2	0.5°	3 hours	Sheffield et al. (2006)
Precipitation	Climate Hazards Group InfraRed Precipitation with Station data (CHIRPS)	0.05°	1 day	Funk et al. (2015)
Soil type	Harmonized World Soil Database version 1.2	~0.083°	n/a	Nachtergaele et al. (2009)
Vegetation type	MODIS Land Cover Maps	~0.004°	n/a	Broxton et al. (2014)
LAI	Global Land Surface Satellite (GLASS)	0.05°	~8 days	Xiao et al. (2013)
GRACE	NASA GSFC Mascons	Irregular	~1 month	Luthcke et al. (2013)

Table 3: Perturbation settings associated with the meteorological forcing data and model parameters. The comprehensive description of model parameters can be found in, e.g., Decker (2015), Ukkola et al. (2016). The spatial correlation error is also applied to forcing data (fourth column). The correlation length of the 0.5° and 0.05° CABLE model (C05, C005) is determined based on covariance analysis (see Sect. 3.2.4).

Forcing/ parameter variables	Description	Perturbation type	Spatially correlated (correlation length)	Standard deviation
Meteorological forcings				
Rainf	Precipitation	Multiplicative	Yes (C05 = 0.7°, C005 = 0.3°)	10 % of the nominal value
Tair	Air temperature	Additive	Yes (C05 = 2.1°, C005 = 2.1°)	2 °C
SW	Shortwave radiation	Multiplicative	Yes (C05 = 2.3°, C005 = 2.3°)	10 % of the nominal value
Model parameters				
$f_{\text{clay}}, f_{\text{sand}}, f_{\text{silt}}$	The fraction of clay, sand, and silt	Multiplicative	No	10 % of the nominal value
f_{sat}	The fraction of the grid cell that is saturated	Additive	No	10 % of the nominal value
q_{sub}	The maximum rate of subsurface drainage assuming a fully saturated soil column	Additive	No	10 % of the nominal value
f_{p}	Tunable parameter controlling drainage speed	Additive	No	10 % of the nominal value
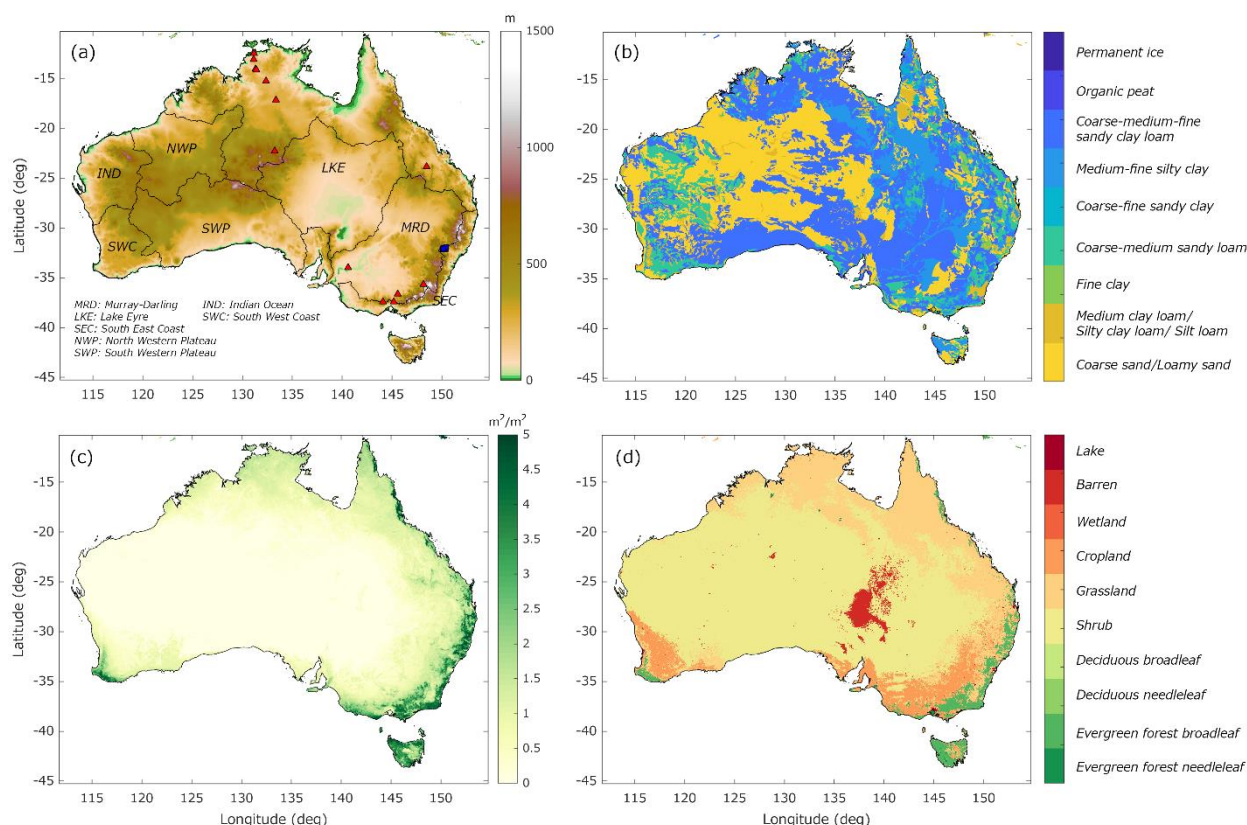
Figure 1: (a) Characteristics of the study area, including elevation, major Australian river basin, and ground observation networks (the Ozenet—red triangle and the SASMAS—blue square). Note that the locations of groundwater sites can be found in Fig. 13. (b – d) The derived 0.05° land cover values for (b) soil class, (c) averaged LAI (used only for demonstration), and (d) vegetation type.
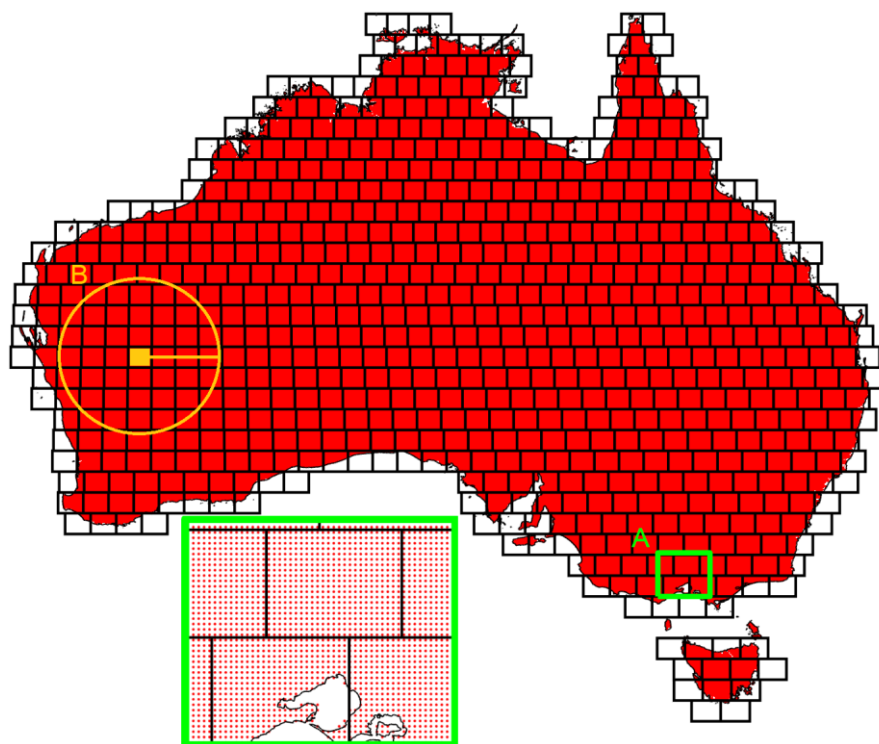
Figure 2: The GRACE GSFC-mascon grid (black rectangles) and the CABLE 0.05° grids (red dots) in Australia. The green inset shows
785   details of rectangle A. The orange circle B shows the number of mascon cells inside a ~3° radius, which are used to update the state variables
inside the center mascon (filled orange). Processing details can be found in Sect. 3.1.
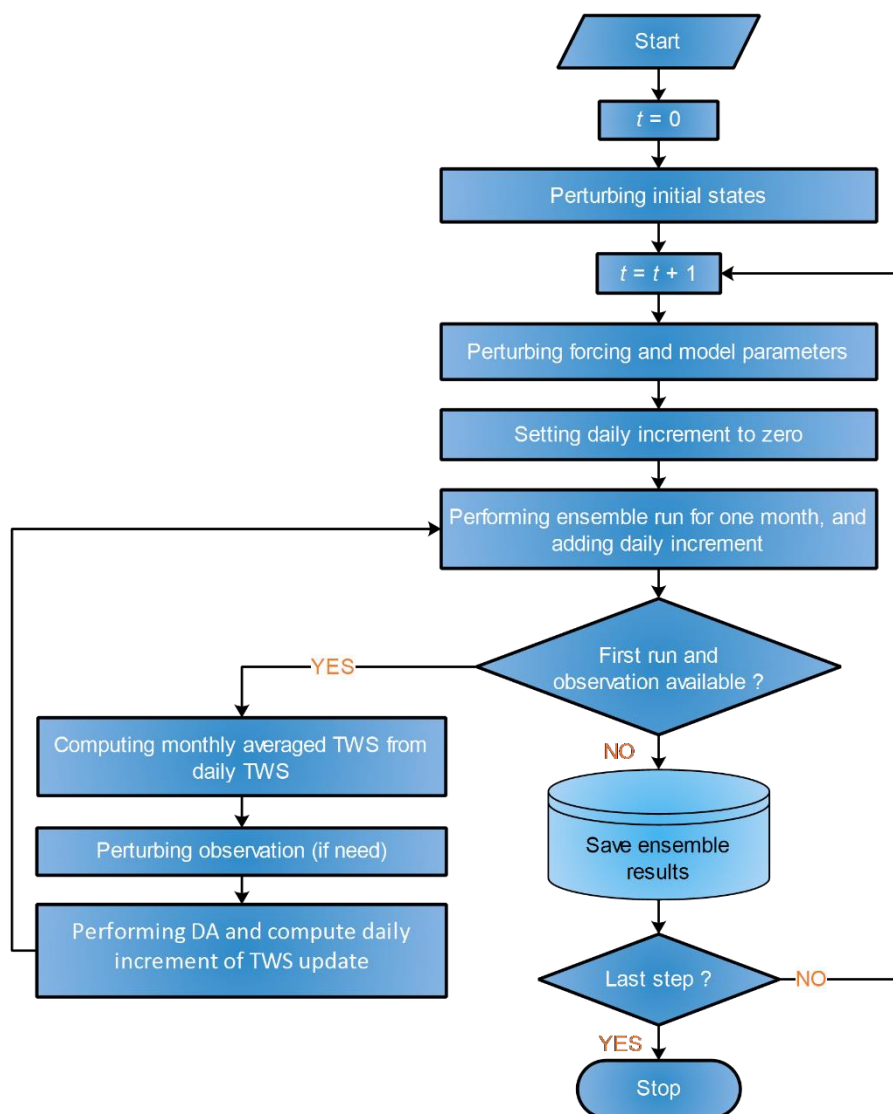
Figure 3: The flow diagram of the GRACE DA process.

790
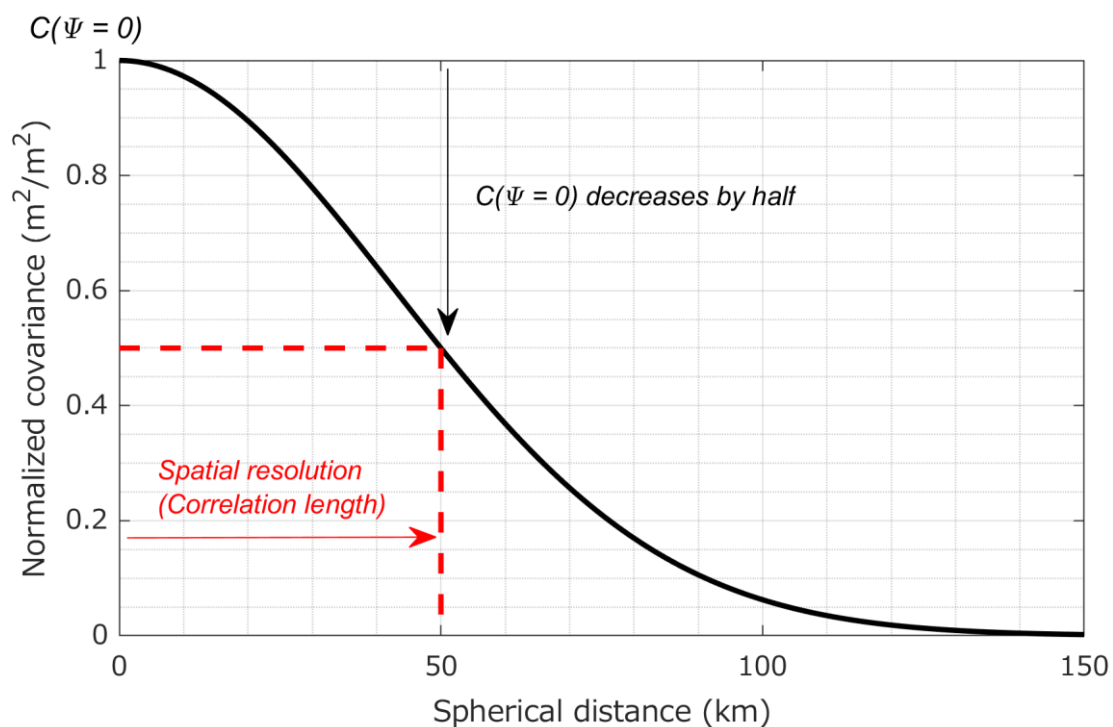
Figure 4: The concept used to determine spatial resolution (correlation length). The spatial resolution is defined to be the spherical distance ψ at which the 0 km covariance (or normalized covariance), $C(\psi = 0)$ decreases by half.
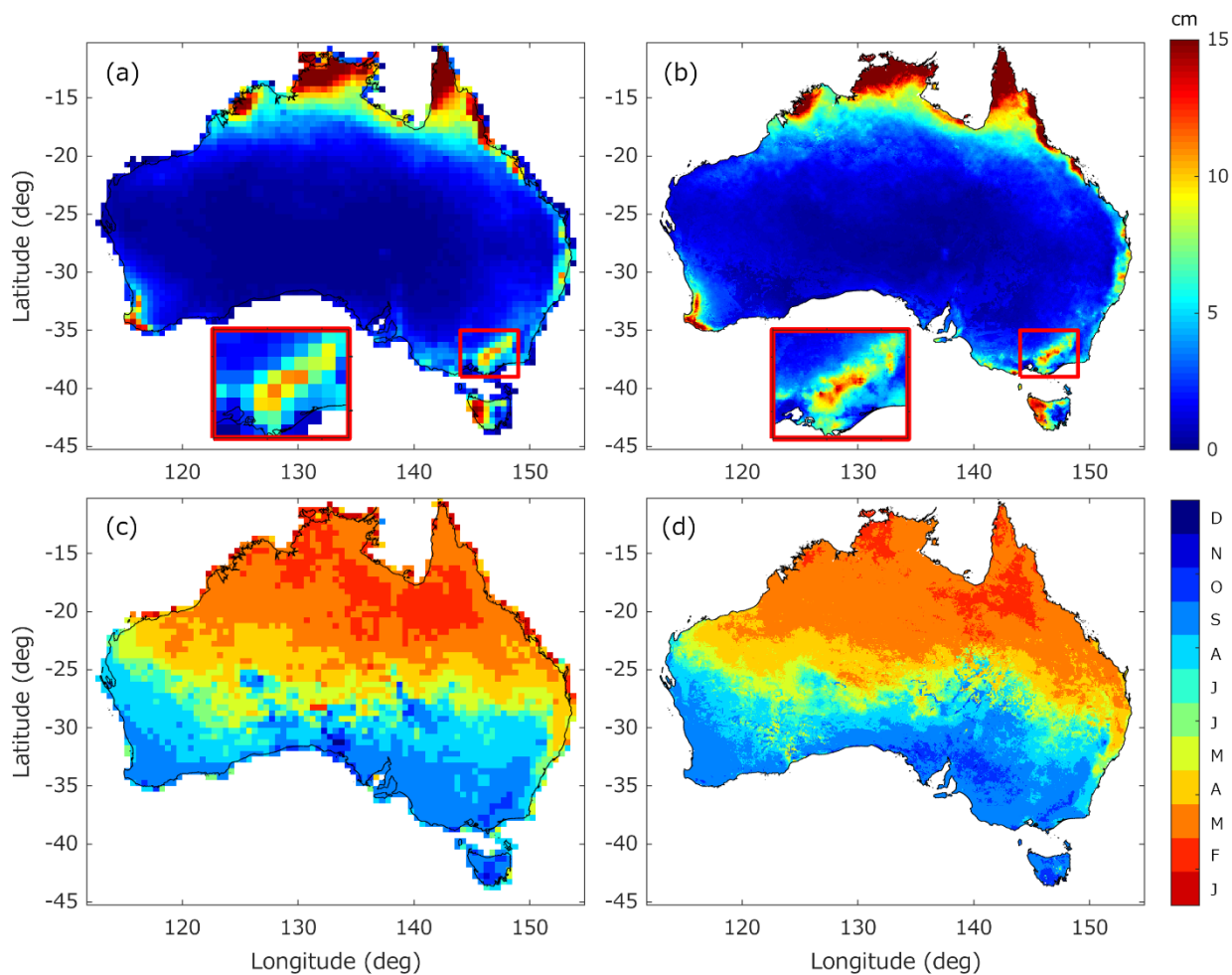
Figure 5: Annual amplitude (top) and phase (bottom) of the TWS estimates computed from CABLE 0.5° (a, c) and CABLE 0.05° (b, d). The insets in (a) and (b) show details in southeast Australia. The unit of the phase is a calendar month, e.g., January (J), December (D).

795
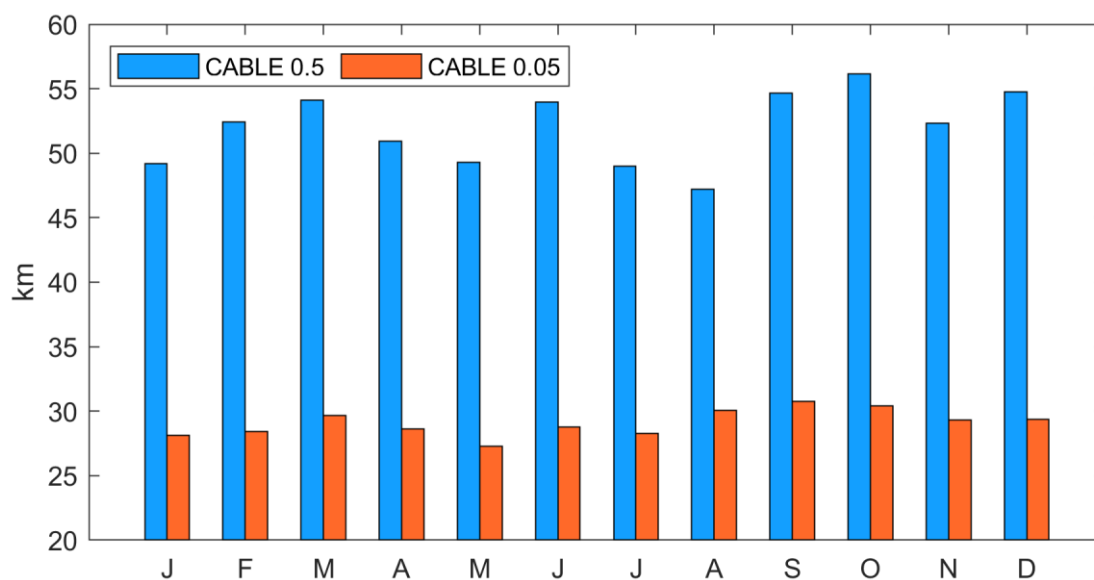
800 **Figure 6:** Monthly average spatial resolutions (correlation lengths) of the TWS estimates derived from CABLE 0.5° and CABLE 0.05° in Australia between 1981 and 2012.
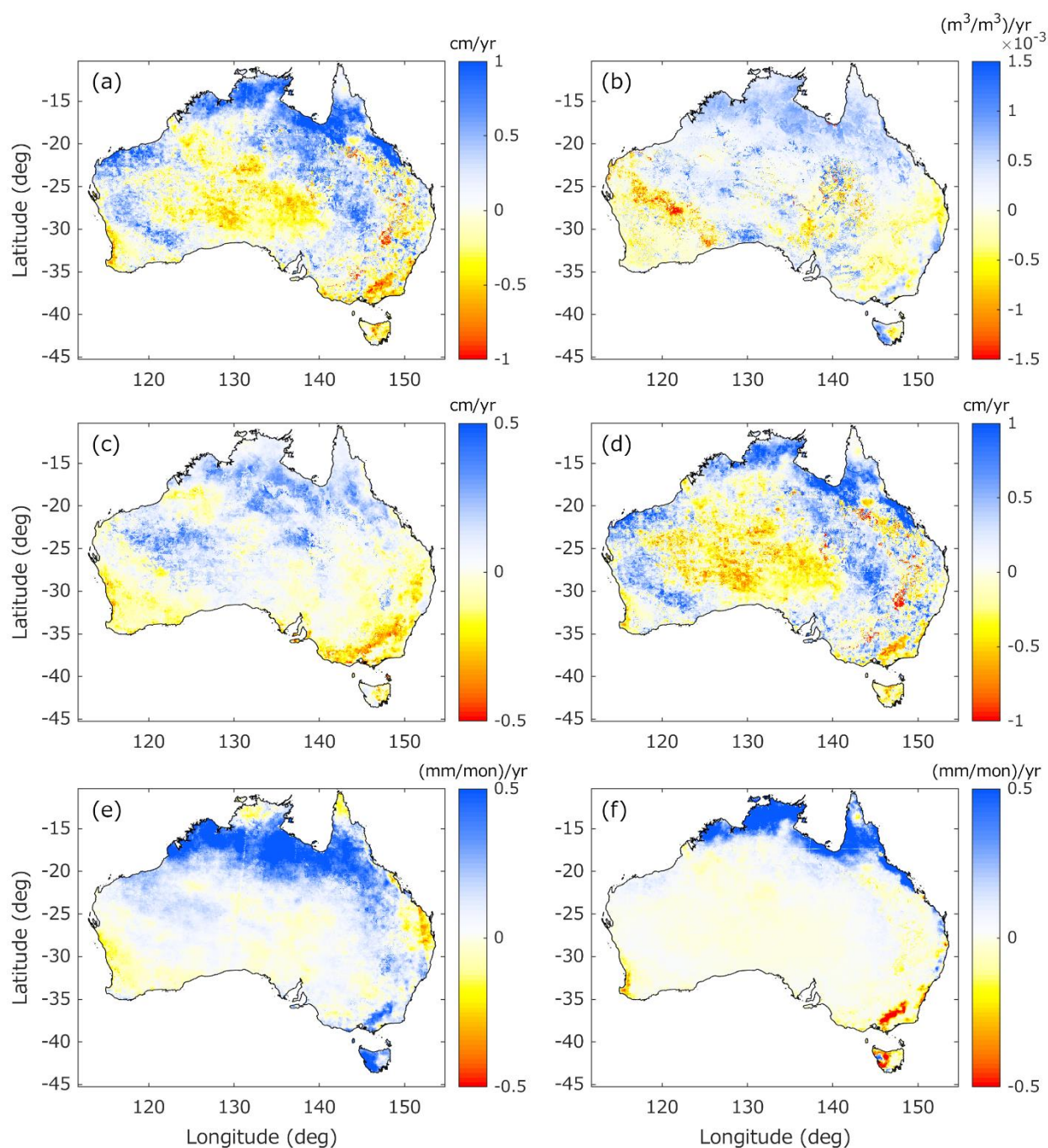
Figure 7: Long-term trends computed from CABLE 0.05° between January 1981 and December 2012: (a) Terrestrial water storage (TWS),
805 (b) Surface (volumetric) soil moisture (SSM), (c) Total soil moisture storage (SMS), (d) Groundwater storage (GWS), (e) Evapotranspiration
(ET), and (f) Total runoff.
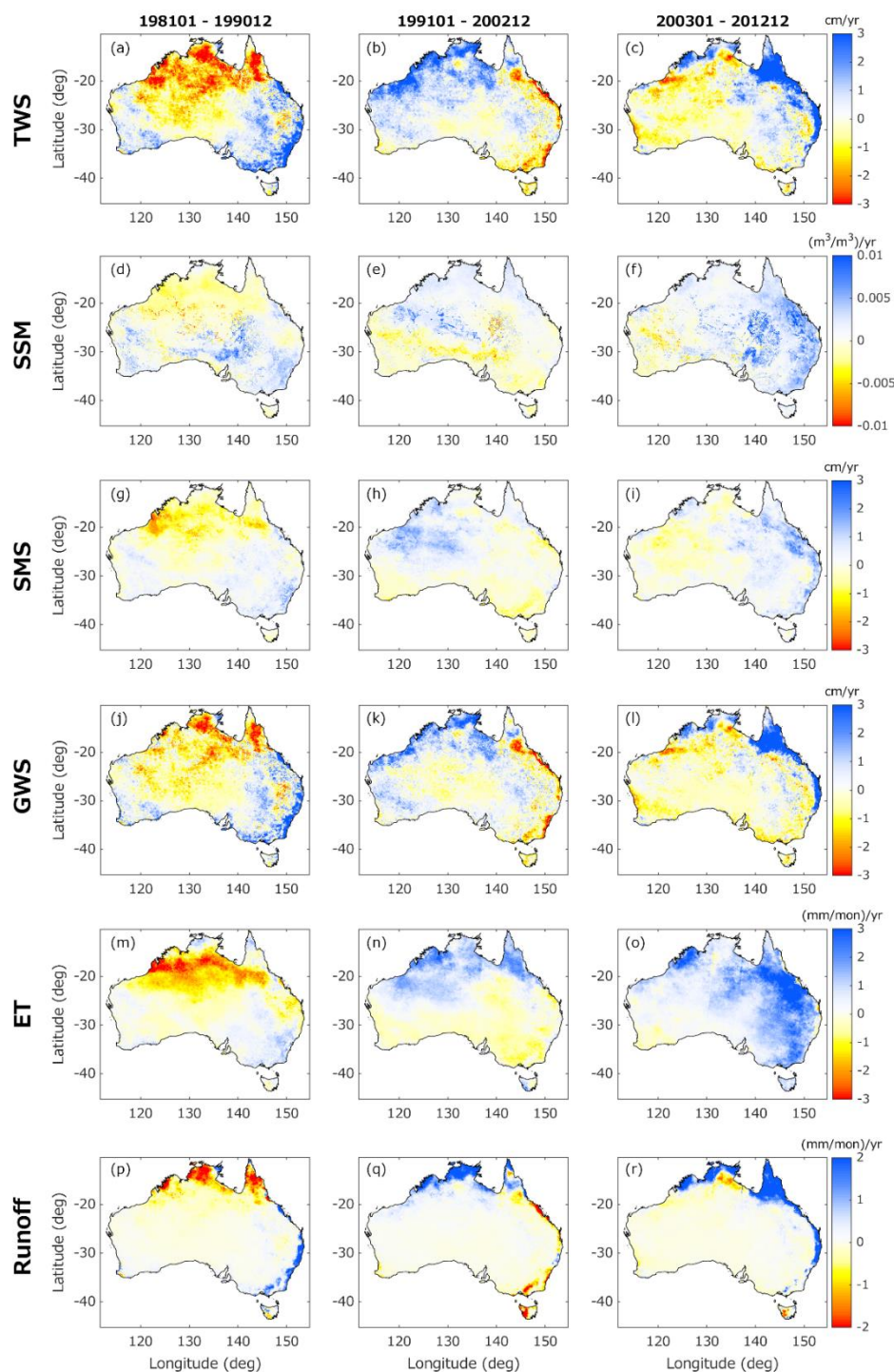
Figure 8: Similar to Fig. 7, but the trends are associated with three different periods, 1981 – 1990 (left column), 1991 – 2002 (middle column), and 2003 – 2012 (right column).
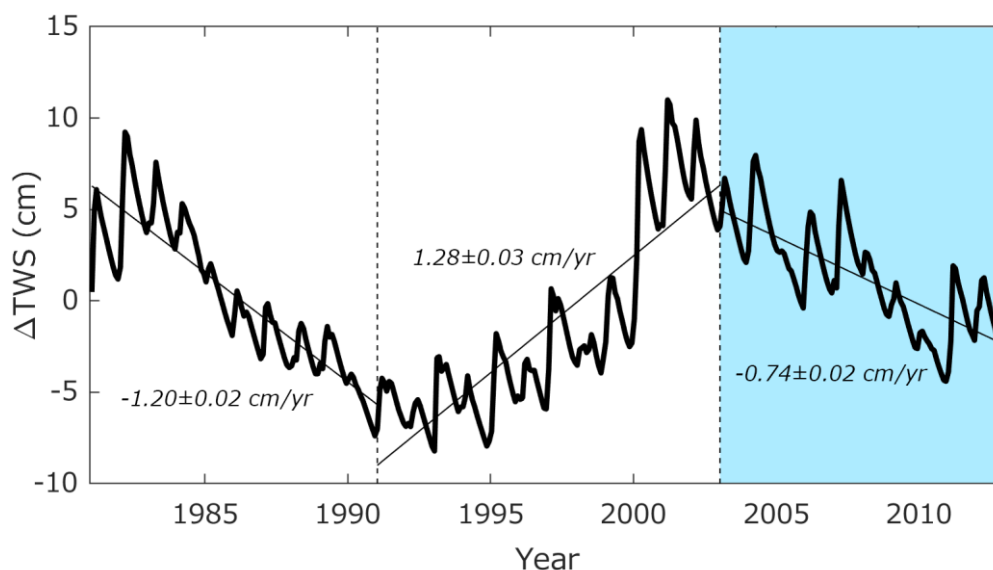
Figure 9: The TWS estimates of the Sandy Desert basin obtained from CABLE 0.05° between January 1981 and December 2012. The long-term trend estimates (cm/yr) in different periods are given. The blue highlight indicates the GRACE period (January 2003 – December 2012).

815
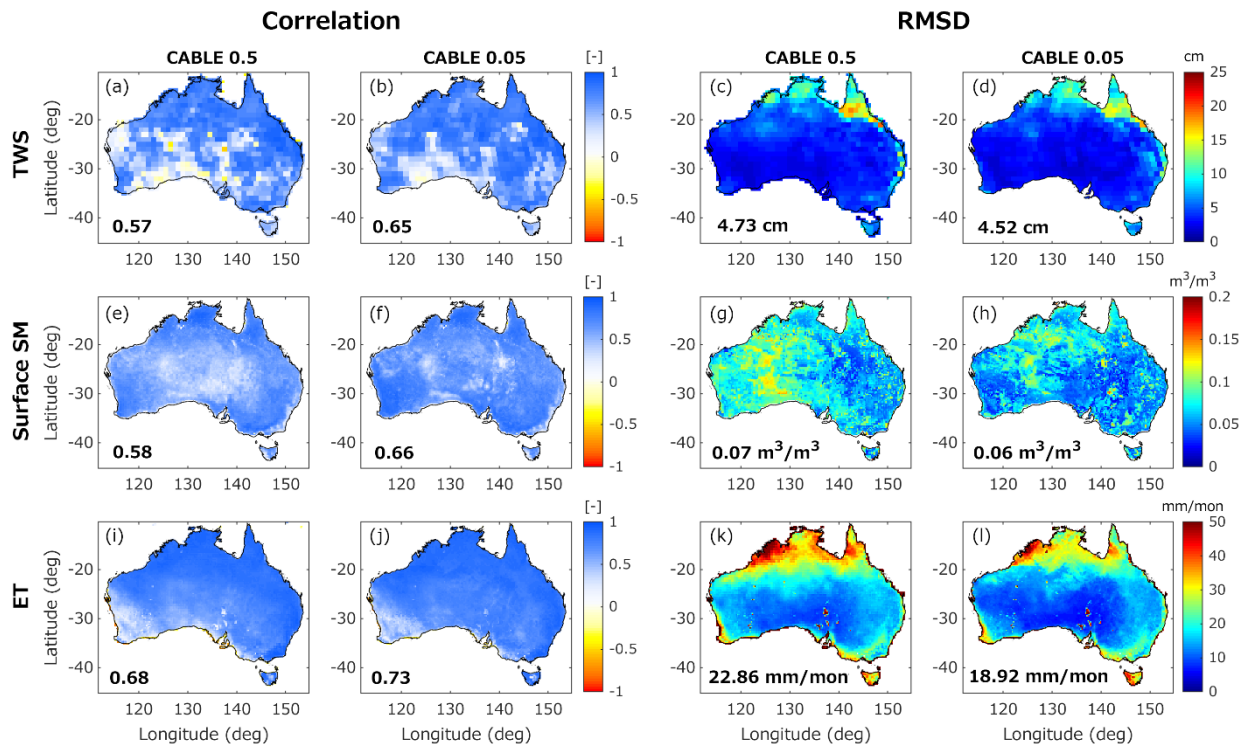
Figure 10: The comparison between CABLE 0.5°/CABLE 0.05° estimates and different remote sensing products in terms of correlation coefficient (left panel) and root-mean-square difference (RMSD, right panel). The terrestrial water storage (TWS, first row), surface soil moisture (Surface SM, second row), and evapotranspiration (ET, bottom row) are compared with GRACE, ESA-CCI, and GLEAM products, respectively. The averaged statistical values (over Australia) associated with each comparison are also given.

820
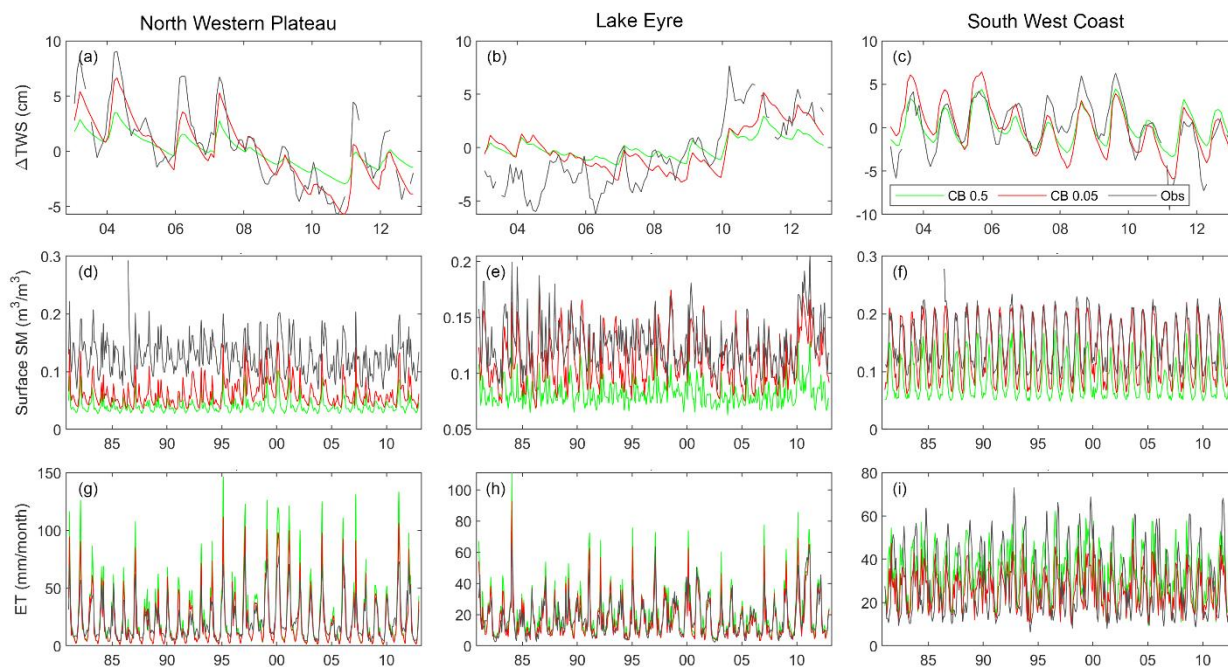
Figure 11: The change in terrestrial water storage (ΔTWS, first row), surface soil moisture (Surface SM, second row), and evapotranspiration (ET, third row) estimated from CABLE 0.5° (CB 0.5), CABLE 0.05° (CB 0.05), and remote sensing observations (Obs) over three different river basins: North Western Plateau (left column), Lake Eyre (middle column), and South West Coast (right column) between 1981 and 2012. The remote sensing observations used for comparison are GRACE (TWS), ESA-CCI (surface SM), and GLEAM (ET).
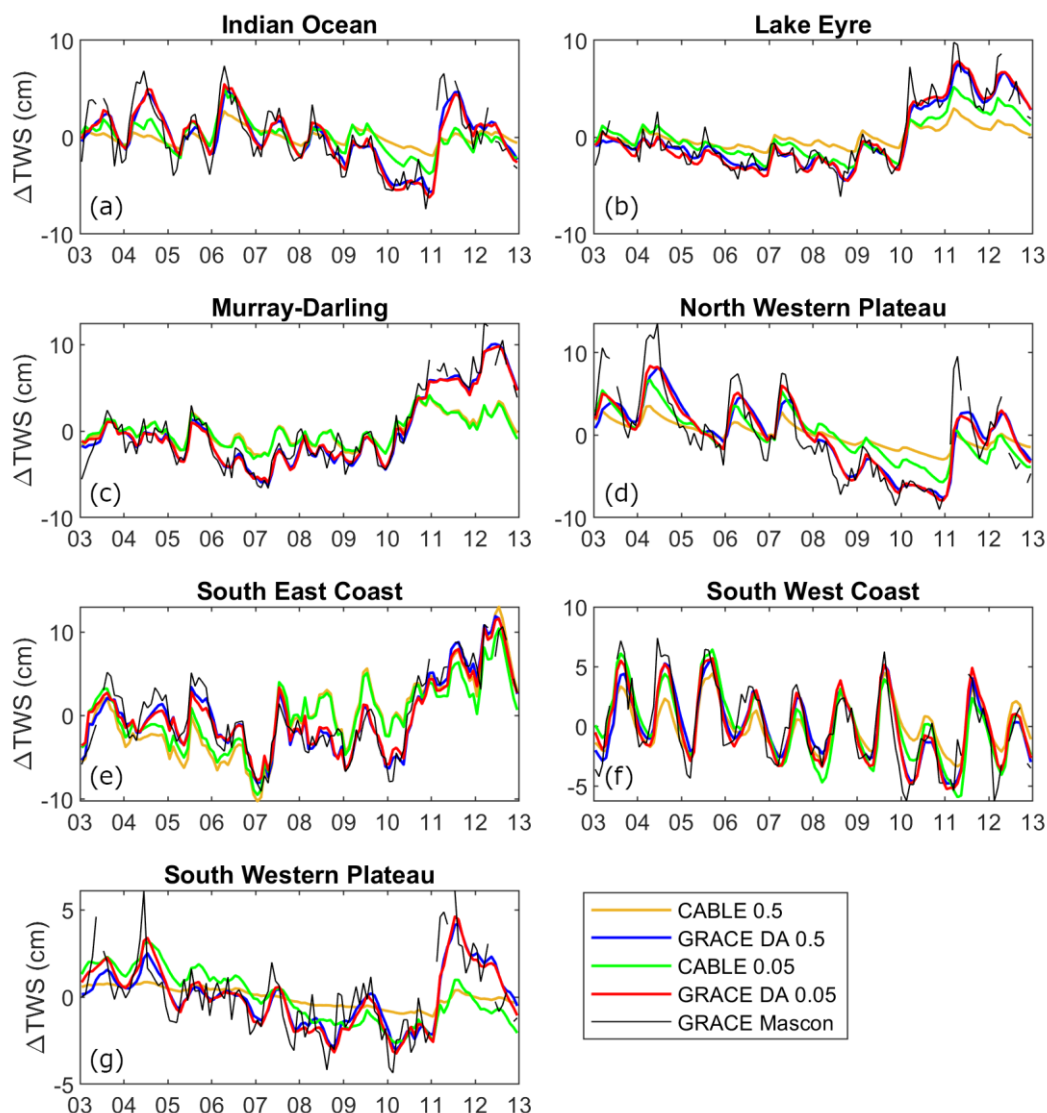
Figure 12: The TWS estimates from case studies CABLE 0.5°, CABLE 0.05°, GRACE DA 0.5°, and GRACE DA 0.05° in various river basins between 2003 and 2012. The GRACE observation is also displayed for comparison. Full descriptions of the case studies are given in Sect. 3.2.5.

830
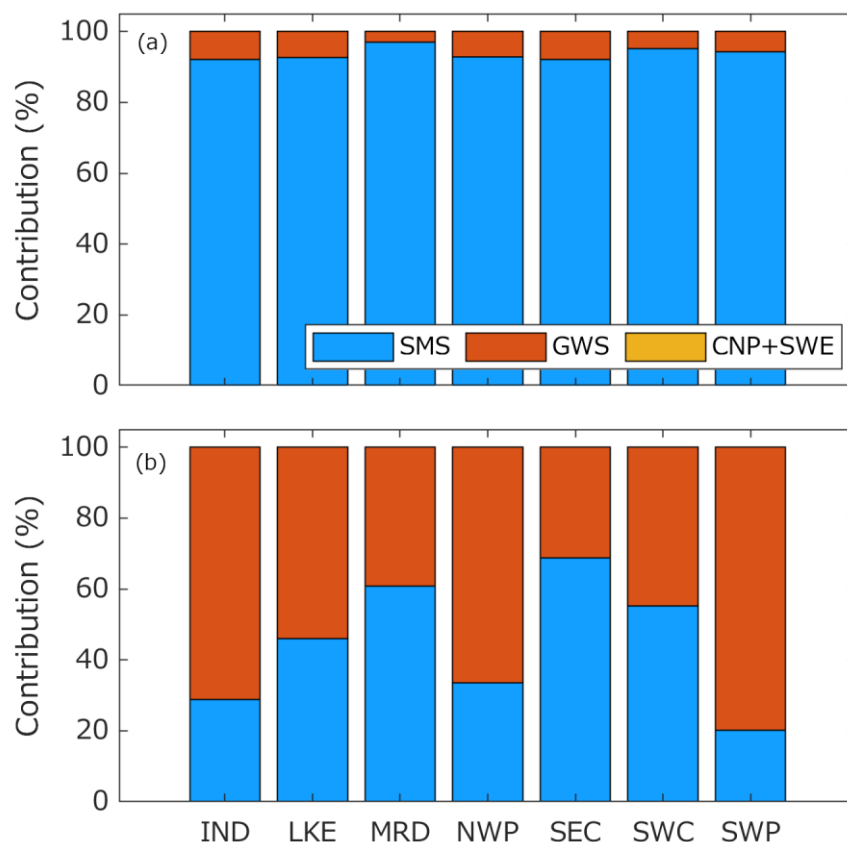
Figure 13: Contributions of different storage components (total soil moisture storage (SMS), groundwater storage (GWS), canopy storage (CNP), and snow water equivalent (SWE)) to the TWS estimates computed from CABLE 0.05° (a) and GRACE DA 0.05° (b) in different river basins. The full names of the river basins are given in Fig. 1a. Contributions of CNP+SWE are negligible in both panels.
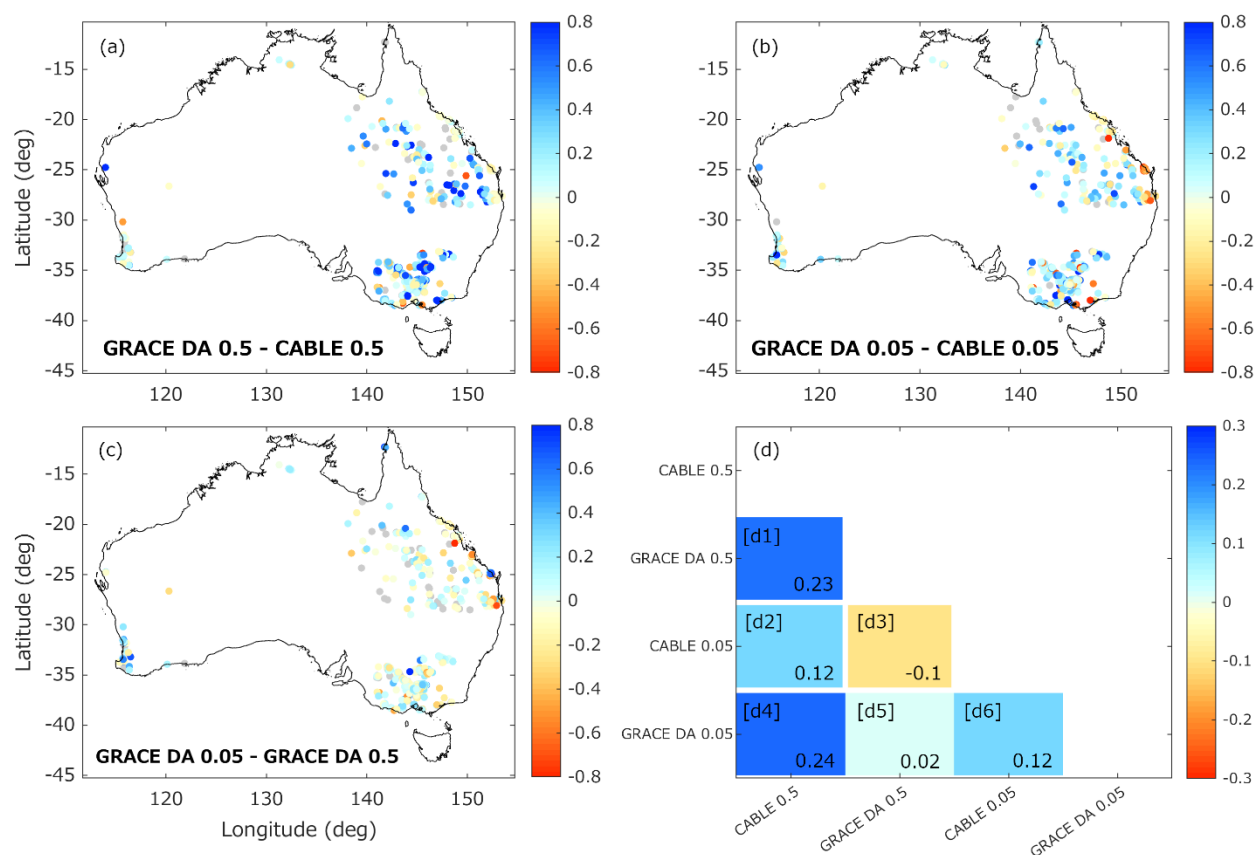
Figure 14: (a – c) Improvements or degradations in correlation values between case study simulations (Sect. 3.2.5) and in situ observations of GWS estimates. (a) GRACE DA 0.5° minus CABLE 0.5°, (b) GRACE DA 0.05° minus CABLE 0.05°, and (c) GRACE DA 0.05° minus GRACE DA 0.5°. The relative performance of each simulation is indicated with blue/red shading: blue indicates the first simulation is better than the second, and red indicates the second is better than the first. Changes that are not significant at the 0.05 level are displayed in grey. (d) The average change in correlation value from each scenario: the vertically-displayed case study minus the horizontally-displayed case study (e.g., d1 represents GRACE DA 0.5° minus CABLE 0.5°, and indicates that the former is significantly better than the latter).

845
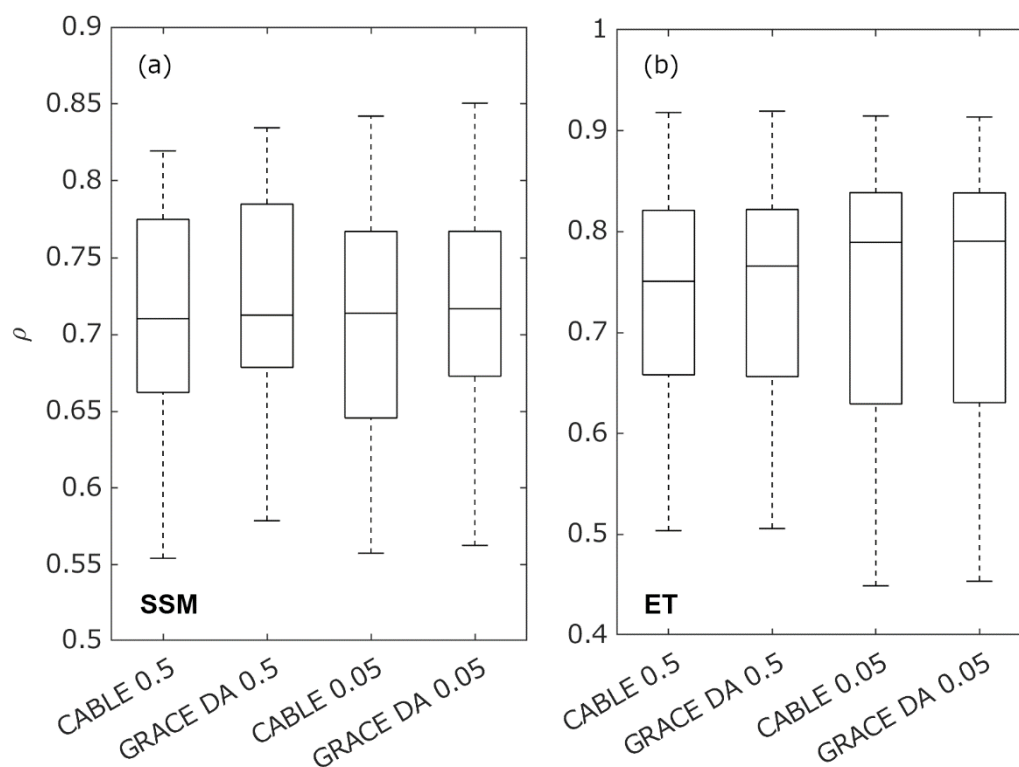
Figure 15: Box and whisker plots showing correlation values between (a) simulation case studies and in situ surface soil moisture, and between (b) simulations and evapotranspiration estimates.